Thermal Jahn–Teller Distortion Changes and Slow Relaxation of Magnetization in Mn(III) Schiff Base Complexes

Chantalaksana Chantarangkul, Apinya Patigo, John C Mcmurtrie, Rodolphe Clérac, Mathieu Rouzières, Silvia Gómez-Coca, Eliseo Ruiz, Phimphaka Harding, David J Harding

Inorganic Chemistry

pubs.acs.org/IC
Article

Thermal Jahn−Teller Distortion Changes and Slow Relaxation of Magnetization in Mn(III) Schiff Base Complexes

Chantalaksana Chantarangkul, Apinya Patigo, John C. McMurtrie, Rodolphe Clérac, Mathieu Rouzières, Silvia Gómez-Coca, Eliseo Ruiz, Phimphaka Harding,* and David J. Harding*

Cite This: *Inorg. Chem.* 2024, 63, 12858−12869
Read Online

ACCESS | Metrics & More | Article Recommendations | Supporting Information

ABSTRACT: The impact that the anion and alkyl group has on the electronic structures and magnetic properties of four mononuclear Mn(III) complexes is explored in $[Mn(salEen\text{-}Br)_2]Y$ (salEen-Br = 2-{[2-(ethylamino)ethylimino]methyl}-4-Br-phenol; Y = ClO_4^- **1** and BF_4^-·1/3CH_2Cl_2 **2**) and $[Mn(salBzen\text{-}Br)_2]Y$ (salBzen-Br = 2-{[2-(benzylamino)ethylimino]methyl}-4-Br-phenol; Y = ClO_4^- **3** and BF_4^- **4**). X-ray structures of $[Mn(salEen\text{-}Br)_2]ClO_4$·0.45$C_6H_{14}$ **1-hexane**, $[Mn(salEen\text{-}Br)_2]BF_4$·0.33$CH_2Cl_2$·0.15$C_6H_{14}$ **2-dcm-hexane**, and **3**−**4** reveal that they crystallize in ambient conditions in the monoclinic $P2_1/c$ space group. Lowering the temperature, **2-dcm-hexane** uniquely exhibits a structural phase transition toward a monoclinic $P2_1/n$ crystal structure determined at 100 K with the unit cell trebling in size. Remarkably, at room temperature, the axially elongated Jahn−Teller axis in **2-dcm-hexane** is poorly defined but becomes clearer at low temperature after the phase transition. Magnetic susceptibility measurements of **1**−**4** reveal that only **3** and **4** show slow relaxation of magnetization with Δ_{eff}/k_B = 27.9 and 20.7 K, implying that the benzyl group is important for observing single-molecule magnet (SMM) properties. Theoretical calculations demonstrate that the alkyl group subtly influences the orbital levels and therefore very likely the observed SMM properties.

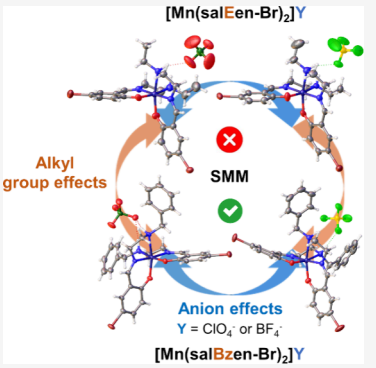

INTRODUCTION

Magnetic materials play an important role in the development of technology in the field of electronic devices such as sensors[1] and storage devices.[2] Single-molecule magnets (SMMs) are molecular nanomagnets that exhibit slow relaxation of magnetization and can potentially be applied to future data storage.[3] The efficiency of SMMs can be determined by the size of the energy barrier (Δ) for spin reversal, which is significantly dominated by the axial zero-field splitting parameter (D) and the total spin (S). The formulas $\Delta = S^2|D|$ and $\Delta = (S^2 - (1/4))|D|$ can be used to approximate Δ for SMMs with integer and noninteger spins, respectively.[4]

Sessoli et al. discovered the first SMM, a mixed valent Mn(III)/Mn(IV) complex $[Mn_{12}O_{12}(CH_3CO_2)_{16}(H_2O)_4]$ or Mn_{12}ac, in 1993.[5] In the initial studies of SMMs, polynuclear Mn complexes were the focus; however, they exhibit poor SMM properties.[6−10] However, in 2007 the Brechin group reported a $[Mn_6]$ complex with a slightly higher Δ_{eff} (86.4 K) than Mn_{12} (Δ_{eff}/k_B = 60 K).[11] The exploration of other 3d and 3d−4f polynuclear complexes subsequently followed.[12−30] Lanthanides were introduced with the aim of stabilizing magnetic coupling between the metal centers while taking advantage of the lanthanides' larger spin−orbit coupling constant to enhance the energy barrier. While a range of molecular systems of unusual shape and magnetic properties have resulted, the most effective designs employ simple linear [M(L)Dy(L)M] {L = 2,2′,2″-(((nitrilotris(ethane-2,1-diyl))tris(azanediyl))tris-(methylene))tris(4-halophenol)} architectures with effective energy barriers of 459 and 600 K for the M = Fe(II) and Co(II) systems, respectively.[31,32]

In 2003, Ishikawa and co-workers reported the first mononuclear SMM based on a lanthanide ion, [TBA][Pc_2Ln] (Pc = pthalocyanine, TBA = tetrabutylammonium, and Ln = Tb, Dy).[33] This led to an explosion of interest in mononuclear complexes of d or f elements as these tend to have more pronounced magnetic anisotropy leading to improved SMM behavior. Lanthanide systems remain popular for studying SMM properties due to the large magnetic anisotropy of the central metal ion, which results in a high relaxation barrier. An excellent example of this is the very large Δ_{eff} (1760 K) found in the dysprosocenium complex, $[Dy(Cp^{ttt})_2][B(C_6F_5)_4]$ (Cp^{ttt}={$C_5H_2{}^tBu_3$-1,2,4} and ^{t}Bu = $C(CH_3)_3$).[34] However, these magnetic materials are very air-sensitive and expensive. In recent years, first-row transition systems have received renewed attention. 3d-block mononuclear SMMs are known in the case of Fe(I/II/III),[35−37] Mn(III),[38−45] Co(II),[46−49] Ni(I/II),[50−52] and Cr(II)[53] systems with researchers looking for compounds

Received: April 1, 2024
Revised: June 6, 2024
Accepted: June 13, 2024
Published: June 27, 2024

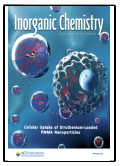

with higher Δ_{eff} values. One method for increasing Δ is to maximize the number of unpaired electrons (higher S), which usually involves using high-spin complexes if the electron configuration is $3d^4$ to $3d^7$. This approach is constrained by D and S being interdependent, and D values typically decrease as S increases. However, octahedral high-spin $3d^4$ Mn(III) complexes with axial elongation due to Jahn−Teller (JT) distortion exhibit a large axial magnetic anisotropy, resulting in large negative D values despite the high S value.[54]

In 2013, Vallejo et al. reported the first example of a mononuclear octahedral Mn(III) SMM, $Ph_4P[Mn(opbaCl_2)(py)_2]$ {$H_4opbaCl_2$ = *N*,*N*′-3,4-dichloro-*o*-phenylenebis(oxamic acid)}. The structure shows axial elongation along the $N_{pyridine}$−Mn(III)−$N_{pyridine}$ axis and magnetic analysis revealed a Δ_{eff} value of 18.1 K.[38] After that, the first mononuclear Mn(III) SMM with a tridentate Schiff base (SB) ligand $[Mn(3\text{-}OEt\text{-}salme)_2]BPh_4$ (salme = *N*-methyl-*N*-(3-aminopropyl)salicylaldiminate), was reported by Realista et al.[45] The structure exhibits a JT elongation along the N_{amine}−Mn−N_{amine} axis and Δ_{eff} for spin reversal of 10.2 K and while lower than that above is in line with other mononuclear Mn(III) SMMs.[38−44] Nevertheless, many questions remain and additional investigations concerning Mn(III) complexes with tridentate SB ligands is warranted.

Herein, four new Mn(III) complexes with tridentate SB ligands, $[Mn(salEen\text{-}Br)_2]$anion (salEen-Br = 2-{[2-(ethylamino)ethylimino]methyl}-4-Br-phenol; anion = ClO_4^- **1** and $BF_4^-\cdot 1/3CH_2Cl_2$ **2**) and $[Mn(salBzen\text{-}Br)_2]$anion (salBzen-Br = 2-{[2-(benzylamino)ethylimino]methyl}-4-Br-phenol; anion = ClO_4^- **3** and BF_4^- **4**), are reported to investigate the electronic structures and the SMM behavior of these mononuclear Mn(III) complexes upon varying the anions and ligands. To provide a deeper understanding, theoretical calculations of all Mn(III) complexes have been utilized to investigate why SMM behavior was observed only in **3** and **4**.

EXPERIMENTAL SECTION

General Remarks. All solvents were of AR grade, and all reactions were conducted in air. All chemicals were purchased from Sigma-Aldrich or TCI Chemicals and used as received. The SC-XRD studies detailed below indicate that the SC-XRD studies detailed below indicate that the chemical formulas for the ethyl complexes are $[Mn(salEen\text{-}Br)_2]ClO_4\cdot 0.45C_6H_{14}$ (termed **1-hexane**) and $[Mn(salEen\text{-}Br)_2]BF_4\cdot 1/3CH_2Cl_2\cdot 0.15C_6H_{14}$ (termed **2-dcm-hexane**). Elemental analysis reveals that the hexane is readily lost and the correct formulas for the bulk samples are $[Mn(salEen\text{-}Br)_2]ClO_4$ **1**, $[Mn(salEen\text{-}Br)_2]BF_4\cdot 1/3CH_2Cl_2$ **2**, $[Mn(salBzen\text{-}Br)_2]ClO_4$ **3**, and $[Mn(salBzen\text{-}Br)_2]BF_4$ **4**. All spectroscopic and magnetic studies were conducted on the bulk samples as detailed below.

CAUTION: Although we experienced no problems when using the perchlorate salts in this study, metal−organic perchlorates are potentially explosive and should be handled with care in small quantities.

Synthesis of HsalEen-Br and HsalBzen-Br Ligands. To a solution of 5-bromosalicyaldehyde (0.1988 g, 1 mmol) in ethanol (3 mL) was added *N*-ethylethylenediamine (0.1503 mL, 1 mmol), which was stirred for 1 h giving a yellow-orange solution.[55−58] HsalBzen-Br was prepared similarly changing *N*-ethylethylenediamine to *N*-benzylethylenediamine (0.1502 mL, 1 mmol).[59] The mixture gives a yellow solution.

Synthesis of $[Mn(salEen\text{-}Br)_2]ClO_4$, 1. $Mn(ClO_4)_2\cdot 6H_2O$ (0.1700 g, 0.5 mmol) was dissolved in water (5 mL) and stirred for 15 min. NEt_3 (0.1390 mL, 1 mmol) was added to a solution of HsalEen-Br made *in situ* (1 mmol in ethanol 3 mL) and solution stirred for 10 min. After that, the HsalEen-Br solution was added dropwise to the Mn solution and stirred overnight. The resulting brown-red solid was filtered and washed with water, ethanol, and diethyl ether. The solid was recrystallized by layering from dichloromethane/hexane, and dark-red crystals were collected after 7 days (170 mg, 49%). Found (calcd. %) for $C_{22}H_{28}Br_2ClMnN_4O_6$ (694.68 g mol^{-1}): C 37.73 (38.04), H 3.81 (4.06), N 8.22 (8.07). ESI^+ found (calcd. *m*/*z*): 595.46 (594.99) $[Mn(salEen\text{-}Br)_2]^+$. IR data (KBr, cm^{-1}; Figure S1): 3274, 3215 (ν_{N-H}); 2966, 2939, 2876 (ν_{C-H}); 1616 ($\nu_{C=N}$); 1518, 1448 ($\nu_{C=C}$); 1383, 1170 (ν_{C-N}); 1296 (ν_{C-O}); 1088, 1060 (ν_{Cl-O}); 974; 933; 800; 731; 681; 621; 567; 457.

Synthesis of $[Mn(salEen\text{-}Br)_2]BF_4\cdot 1/3CH_2Cl_2$, 2. $[Mn(salEen\text{-}Br)_2]BF_4$ **2** was prepared using a similar procedure to **1** but using $Mn(OAc)_3\cdot 2H_2O$ (0.1354 g, 0.5 mmol) instead of $Mn(ClO_4)_2\cdot 6H_2O$. An excess of $NaBF_4$ (0.2192 g, 2 mmol) in ethanol (10 mL) and water (2 mL) was stirred for 15 min and then added to the Mn(III) solution to yield $Mn(BF_4)_3$ after 30 min. The deprotonated HsalEen-Br solution was added to the Mn(III) solution and stirred for 3 h. The dark-brown solid that formed was filtered and dried. The solid was recrystallized by layering from dichloromethane/hexane, and dark-red crystals were collected (180 mg, 53%). Found (calcd. %) for $C_{22}H_{28}BBr_2F_4MnN_4O_2\cdot 1/3CH_2Cl_2$ (710.07 g mol^{-1}): C 37.41 (37.77), H 4.01 (4.07), N 8.08 (7.89). ESI^+ found (calcd. *m*/*z*): 595.45 (594.99) $[Mn(salEen\text{-}Br)_2]^+$. IR data (KBr, cm^{-1}; Figure S1): 3301, 3256 (ν_{N-H}); 2970, 2939, 2876 (ν_{C-H}); 1618 ($\nu_{C=N}$); 1518, 1448 ($\nu_{C=C}$); 1379, 1167 (ν_{C-N}); 1294 (ν_{C-O}); 1055 (ν_{B-F}); 970; 935; 798; 725; 677; 638; 565; 457.

Synthesis of $[Mn(salBzen\text{-}Br)_2]ClO_4$, 3. $[Mn(salBzen\text{-}Br)_2]ClO_4$ **3** was prepared using a similar procedure to **1** but changing HsalEen-Br to HsalBzen-Br and using ethanol only. After stirring overnight, brown-orange solid was filtered and dried. The solid was recrystallized by layering from dichloromethane/hexane, and red crystals were collected (215 mg, 53%). Found (calcd. %) for $C_{32}H_{32}Br_2ClMnN_4O_6$ (818.82 g mol^{-1}): C 46.61 (46.94), H 3.83 (3.94), N 7.15 (6.84). ESI^+ found (calcd. *m*/*z*): 719.66 (719.03) $[Mn(salBzen\text{-}Br)_2]^+$. IR data (KBr, cm^{-1}; Figure S1): 3279, 3223 (ν_{N-H}); 3060, 3026, 2955 (ν_{C-H}); 1612 ($\nu_{C=N}$); 1518, 1450 ($\nu_{C=C}$); 1387, 1175 (ν_{C-N}); 1296 (ν_{C-O}); 1127, 1086 (ν_{Cl-O}); 984; 924; 827; 737; 679; 621; 544; 449.

Synthesis of $[Mn(salBzen\text{-}Br)_2]BF_4$, 4. $[Mn(salBzen\text{-}Br)_2]BF_4$ **4** was prepared using a similar procedure to **2** but changing $NaBF_4$ to $[NH_4]BF_4$ (0.2070 g, 2 mmol) and HsalEen-Br to HsalBzen-Br. This reaction was synthesized using ethanol only. The brown solid was filtered and dried. After recrystallizing by layering from dichloromethane/hexane, the dark-brown crystals were collected (254 mg, 63%). Found (calcd. %) for $C_{32}H_{32}BBr_2F_4MnN_4O_2$ (806.17 g mol^{-1}): C 47.40 (47.67), H 4.06 (4.00), N 7.29 (6.95). ESI^+ found (calcd. *m*/*z*): 719.46 (719.03) $[Mn(salBzen\text{-}Br)_2]^+$. IR data (KBr, cm^{-1}; Figure S1): 3299, 3254 (ν_{N-H}); 3063, 3028, 2951 (ν_{C-H}); 1612 ($\nu_{C=N}$); 1518, 1452 ($\nu_{C=C}$); 1387, 1175 (ν_{C-N}); 1294 (ν_{C-O}); 1076 (ν_{B-F}); 982; 928; 827; 739; 679; 638; 521; 456.

X-ray Crystallography. The diffraction data of **1-hexane**, **2-dcm-hexane**, and **3**−**4** were collected with CuKα radiation (λ = 1.54184 Å) using a Rigaku SuperNova (HyPix-3000 detector)[60] diffractometer. Data reduction, scaling, and absorption corrections were performed in CrysAlisPro.[61] The structures were solved, and the space groups were determined by intrinsic phasing using ShelXT[62] and refined by full matrix least-square minimization on F^2 using SHEXL.[63] All non-hydrogen atoms were refined anisotropically, with the exception of **1-hexane** and **2-dcm-hexane** where disorder in the anion was modeled isotropically for the minor component. Compound **1-hexane** contains hexanes, while **2-dcm-hexane** contains CH_2Cl_2 and hexane. In both cases, the hexane is highly disordered and could not be modeled and was masked using the standard routine in Olex2. In the case of **2-dcm-hexane**, above 100 K the CH_2Cl_2 molecule was also masked due to severe disorder. Hydrogen atoms were included in calculated positions and refined with isotropic thermal parameters, which were 1.2× or 1.5× the equivalent isotropic thermal parameters of their parent carbon atoms. All pictures were generated with Olex2. Crystallographic data of **1-hexane**, **2-dcm-hexane**, and **3**−**4** has been submitted to the Cambridge Crystallographic Data Centre (CCDC) under 2344242−2344250.

Physical Measurements. Infrared spectra were collected as ATR on a Bruker Tensor 27 FT-IR spectrometer with OPUS software in the range of 400−4000 cm^{-1}. UV−vis spectra were measured with a T80

https://doi.org/10.1021/acs.inorgchem.4c01317
Inorg. Chem. 2024, 63, 12858−12869

Series UV/vis Double Beam Spectrophotometer by PG Instruments, Ltd., in the range of 200−800 nm. A EuroVector EA3000 analyzer was utilized for elemental analysis. ESI-MS were carried out on a Bruker Amazon X LCMS Mass Spectrometer. Thermogravimetric analysis was measured with a Mettler Toledo TGA/DSC1 in the range of 35−250 °C. Magnetic measurements were performed on a Quantum Design MPMS-XL magnetometer and PPMS-II susceptometer between 1.8 and 300 K and dc magnetic fields ranging from −9 to +9 T. The ac magnetic susceptibility measurements were performed in an oscillating ac field of 1 to 6 Oe with frequencies between 0.1 and 10,000 Hz and various dc fields (including zero). The measurements were carried out on polycrystalline samples of **1**−**4** suspended in mineral oil and introduced in a sealed polyethylene bag. The magnetic susceptibilities were corrected for the sample holder, the mineral oil, and the intrinsic diamagnetic ($-0.5 \times MW \times 10^{-6}$ cm^3/mol; MW being the molecular weight of the complex as determined from elemental analysis of the bulk samples) contributions.

Theoretical Calculations. Complete active space self-consistent field (CASSCF)[64] and second-order N-electron valence state perturbation theory (NEVPT2) calculations[65] were performed using ORCA (5.0.3 version)[66,67] with a (4,5) active space and the def2-TZVPP basis set, including the auxiliary basis set for correlation and Coulomb fitting, for all the atoms.[68,69] The spin−orbit effects were included using the quasi-degenerate perturbation theory (QDPT). All 5 quintuplets, 45 triplets, and 50 singlets were calculated and included in the state average. These calculations were employed to analyze the main magnetic descriptors including the axial and rhombic zero-field splitting parameters (D and E), the magnetic susceptibility (χ), and the magnetization (M) of all complexes.[70,71] The X-ray crystallographic structures of **1**−**4** with and without the anion (**1**$^+$−**4**$^+$) at 150 K were employed for the calculations.

RESULTS AND DISCUSSION

Synthesis. The complexes were synthesized by adding a deprotonated HsalRen-Br solution to a solution of $Mn(ClO_4)_2 \cdot 6H_2O$ or $Mn(OAc)_3 \cdot 2H_2O$. In the case of **2** and **4**, before adding the HsalRen-Br solution, anion exchange with $NaBF_4$ or $[NH_4]BF_4$ was performed (see Scheme 1). Overnight stirring resulted in red-brown solids that were purified by recrystallization from dichloromethane/hexane, yielding deep-red crystals within a week.

Scheme 1. Synthesis of [Mn(salRen-Br)$_2$]Anion (R = Ethyl or Benzyl and Anion = ClO_4^- or BF_4^-) 1−4

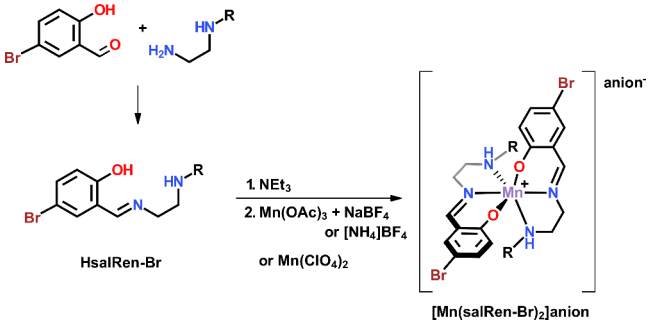

IR and UV−Vis Spectroscopic Studies. The IR spectra of **1**−**4** show the small peaks around 3215−3301 cm^{-1} assignable to N−H stretching. The sharp and strong peaks at 1612−1618 and 1448−1452 cm^{-1} were assigned to the C═N and C═C stretches of the salRen-Br ligand. The anion stretches were found at 1088−1127 and 1055−1076 cm^{-1} for ClO_4^- and BF_4^-, respectively (Figure S1).[56,72,73] The UV−vis spectra in dichloromethane show two absorption regions consistent with a $\pi \rightarrow \pi^*$ transition around 320−360 nm and a ligand to metal charge transfer (LMCT) around 400−440 nm, likely due to the phenolate oxygen p_π to d_π^* metal orbitals by analogy with similar Mn(III) complexes (Figure S2).[72]

Structural Studies. X-ray crystallographic studies of $[Mn(salEen\text{-}Br)_2]Y$ (Y = ClO_4^- **1-hexane** and BF_4^- **2-dcm-hexane**) and $[Mn(salBzen\text{-}Br)_2]Y$ (Y = ClO_4^- **3** and BF_4^- **4**) crystallized from dichloromethane/hexane have been studied at low (100 and/or 150 K) and high (280, 290, or 300 K) temperatures on the same crystal. As noted in the experimental, **1-hexane** contains additional hexane molecules, which have been masked in the structures. Complex **2-dcm-hexane** contains both CH_2Cl_2 and hexane molecules, which have been masked in all structures except that at 100 K, where a single molecule of CH_2Cl_2 is readily identifiable. In both cases, the hexane appears to be readily lost as shown by elemental analysis. The cell volume and crystallographic data are given in Table 1. In all cases, the Mn(III) center has a distorted octahedral geometry with two N_2O donors from the SB ligand with the oxygen donor atoms *cis* to each other and the imine nitrogen donor atoms *trans*, as shown in Figure 1. The complexes crystallize in ambient conditions in the monoclinic space group $P2_1/c$. Lowering the temperature, uniquely **2-dcm-hexane** exhibits a structural phase transition toward a monoclinic $P2_1/n$ crystal structure determined at 100 K with the unit cell trebling in size. The phase transition between 150 and 100 K appears to be due to the concomitant appearance of huge Jahn−Teller effects at all three Mn(III) centers and the ordering of the dichloromethane molecule in the lattice (Figure 1a). Note that the dichloromethane is present in the structures at 150 and 290 K, as shown by the thermogravimetric analysis (Figure S3), but is masked due to significant disorder. Further details concerning this phase transition are discussed below. The Mn−N/O bond distances at high and low temperatures are shown in Figure 2 and Figure S4.

To best describe the changes that occur in the structures, the ligand containing O1, N1, and N2 is termed L1 while that containing O2, N3, and N4 is defined as L2. Generally, in Mn(III) complexes with an N_4O_2 donor set, the ligand favors Jahn−Teller (JT) distortion of the Mn(III) ion center with *trans* donor atoms.[45,73,74] In this work, the JT axis is in most cases readily identifiable from the differences in the Mn−N/O bond distances between the two coordinated ligands, as shown in Figure 2 and Table 2. At both low and high temperatures, **3** and **4** exhibit an elongated Jahn−Teller direction along the O2−Mn1−N4 axis, the bond lengths being 0.053(3)−0.227(3) Å longer than that of the O1−Mn1−N2 axis (L1 ≠ L2). In contrast, in **1-hexane**, the JT axis is not defined at 290 K (L1 = L2). However, it becomes more visible at 150 K due to the longer bonds on the O2−Mn1−N4 axis than on the O1−Mn1−N2 axis by 0.041(3)−0.064(3) Å (L1 ≠ L2), suggesting that the JT axis is positioned along the former axis. Interestingly, the difference between the two ligands is not as large as that found in **3** and **4**. This more pronounced elongation of the Jahn−Teller axes in **3** and **4** may be a contributing factor in the improved SMM performance in **3** and **4** compared to complexes **1** and **2** (*vide infra*). Nevertheless, in all three complexes **1-hexane**, **3**, and **4**, the Jahn−Teller axes become clearer upon cooling, as illustrated in Figure 2a,c,d and Table 3.

The exception is **2-dcm-hexane**. At 290 K, the O2−Mn1−N4 bonds are slightly longer than in the O1−Mn1−N2 axis by 0.027(5)−0.049(4) Å (L1 ≠ L2), suggesting that the JT axis is located along the O2−Mn1−N4 axis and mirroring the results for **1-hexane** at 150 K. However, upon cooling, the Mn-L1 distances increase while the Mn-L2 distances decrease (Figure

https://doi.org/10.1021/acs.inorgchem.4c01317
Inorg. Chem. 2024, 63, 12858−12869

Table 1. Crystallographic Data of 1-hexane, 2-dcm-hexane, and 3−4

	$[Mn(salEen\text{-}Br)_2]ClO_4$, 1-hexane		$[Mn(salEen\text{-}Br)_2]BF_4$, 2-dcm-hexane		
	150 K	290 K	100 K	150 K	290 K
formula	$C_{22}H_{28}Br_2ClMnN_4O_6{\cdot}0.45C_6H_{14}$		$C_{22}H_{28}BBr_2F_4MnN_4O_2{\cdot}0.33CH_2Cl_2{\cdot}0.15C_6H_{14}$		
molecular weight (g/mol)	733.47		725.59	723.00	
space group	$P2_1/c$	$P2_1/c$	$P2_1/n$	$P2_1/c$	$P2_1/c$
crystal system	monoclinic	monoclinic	monoclinic	monoclinic	monoclinic
a (Å)	10.86725(13)	10.89895(16)	10.80230(10)	10.82029(12)	10.8941(3)
b (Å)	26.3107(3)	26.7292(3)	26.3098(3)	26.3661(2)	26.6789(5)
c (Å)	10.86267(14)	10.92248(18)	29.6274(4)	10.74793(16)	10.8037(3)
α (deg)	90	90	90	90	90
β (deg)	113.4025(15)	112.9548(18)	93.7050(10)	113.0765(15)	112.624(3)
γ (deg)	90	90	90	90	90
volume (Å^3)	2850.41(7)	2929.97(8)	8402.70(17)	2820.91(7)	2898.41(14)
Z	4	4	12	4	4
μ (mm^{-1})	8.307	8.082	7.730	7.078	7.420
reflections collected	22,668	23,050	67,619	22,377	21,186
independent reflections, R_{int}	5161, 0.0652	5209, 0.0513	15129, 0.0844	4955, 0.0565	5155, 0.0681
final R indexes $[I \geq 2\sigma(I)]$ R_1, wR_2	0.0454, 0.1214	0.0425, 0.1248	0.0580, 0.1705	0.0471, 0.1308	0.0539, 0.1677
CCDC no.	2344243	2344242	2344246	2344245	2344244

	$[Mn(salBzen\text{-}Br)_2]ClO_4$, **3**		$[Mn(salBzen\text{-}Br)_2]BF_4$, **4**	
	150 K	280 K	150 K	300 K
formula	$C_{32}H_{32}Br_2ClMnN_4O_6$		$C_{32}H_{32}BBr_2F_4MnN_4O_2$	
molecular weight (g/mol)	818.82		806.17	
space group	$P2_1/c$	$P2_1/c$	$P2_1/c$	$P2_1/c$
crystal system	monoclinic	monoclinic	monoclinic	monoclinic
a (Å)	13.4080(2)	13.45546(16)	14.9981(2)	15.0334(2)
b (Å)	21.2369(3)	21.4497(3)	21.2163(2)	21.5244(2)
c (Å)	11.53710(10)	11.63964(15)	11.02250(10)	11.0818(2)
α (deg)	90	90	90	90
β (deg)	94.0520(10)	94.3172(12)	109.1180(10)	108.5260(10)
γ (deg)	90	90	90	90
volume (Å^3)	3276.91(7)	3349.86(8)	3313.96(6)	3400.08(8)
Z	4	4	4	4
μ (mm^{-1})	7.306	7.147	6.570	6.404
reflections collected	26,151	26,552	26,436	26,768
independent reflections, R_{int}	5977, 0.0857	6121, 0.0506	6064, 0.0459	6222, 0.0515
final R indexes $[I \geq 2\sigma(I)]$ R_1, wR_2	0.0494, 0.1453	0.0477, 0.1476	0.0419, 0.1113	0.0537, 0.1476
CCDC no.	2344248	2344247	2344250	2344249

2b and Table 3), such that at 150 K, the JT axis is now undetectable (L1 = L2). Cooling further to 100 K causes a phase transition and symmetry breaking with the appearance of the three independent Mn centers and the ordering of the dichloromethane molecule in the unit cell. We have undertaken measurements on six different crystals from three different batches, observing the same behavior for all samples. At this temperature, the Mn-L1 and Mn-L2 bonds are now clearly different with the JT axes positioned along the O2−Mn1−N4, O4−Mn2−N8, and O6−Mn3−N12 axes with differences between the two ligands of 0.124(3)−0.196(4), 0.143(3)−0.182(3), and 0.088(3)−0.106(3) Å, respectively.

Interestingly, the BF_4^- complexes show greater changes in the Mn−L bond lengths than the ClO_4^- complexes upon changing the temperature, as shown in Table 3. The fact that **1-hexane** does not contain CH_2Cl_2 in the lattice despite the very similar molecular volumes of the two anions (ClO_4^- 55 Å^3 and BF_4^- 53 Å^3)[75] is unexpected. However, given that **1-hexane** does not exhibit a phase transition above 150 K, it would seem that it is the ordering of the solvent in the lattice that drives the subsequent appearance of the Jahn−Teller axes during the phase transition that occurs in **2-dcm-hexane**. This is supported by the observations concerning **4** in which there is no phase transition or solvent in the lattice, presumably due to the larger benzyl group. Interestingly, $[Fe(1\text{-}bpp\text{-}S\text{-}iPr)_2][anion]_2{\cdot}MeCN$ {1-bpp-SiPr = 2,6-di(pyrazol-1-yl)-4-isopropylthiopyridine} with BF_4^- and ClO_4^- exhibit starkly different spin crossover properties emphasizing how small differences can often lead to unexpected outcomes.[76]

Magnetic Properties. From direct-current (dc) measurements, the evolutions of the χT product in temperature show a clear plateau above 50 K with values at 300 K of 3.1, 3.0, 2.9, and 3.0 cm^3 K/mol for **1**−**4** (Figure 3 and left part of Figure S5). These values are in good agreement with an $S = 2$ (high spin) ground state typical of mononuclear Mn(III) complexes.[38−45] Lowering the temperature below 50 K, the χT values decrease, in accordance with the presence of magnetic anisotropy as expected for anisotropic Mn(III) metal ions. The χT values reach 2.1, 1.9, 1.9, and 2.0 cm^3 K/mol at 1.85 K and 0.1 T for **1**−**4**. The field-dependent magnetization of all complexes was measured below 8 K. The magnetization of these mononuclear Mn(III) complexes does not clearly saturate even at 7 T and 1.85 K, showing a continuous slow increase at high field above 3 T (Figure 3 inset and right part of Figure S5). This field behavior is

https://doi.org/10.1021/acs.inorgchem.4c01317
Inorg. Chem. 2024, 63, 12858−12869

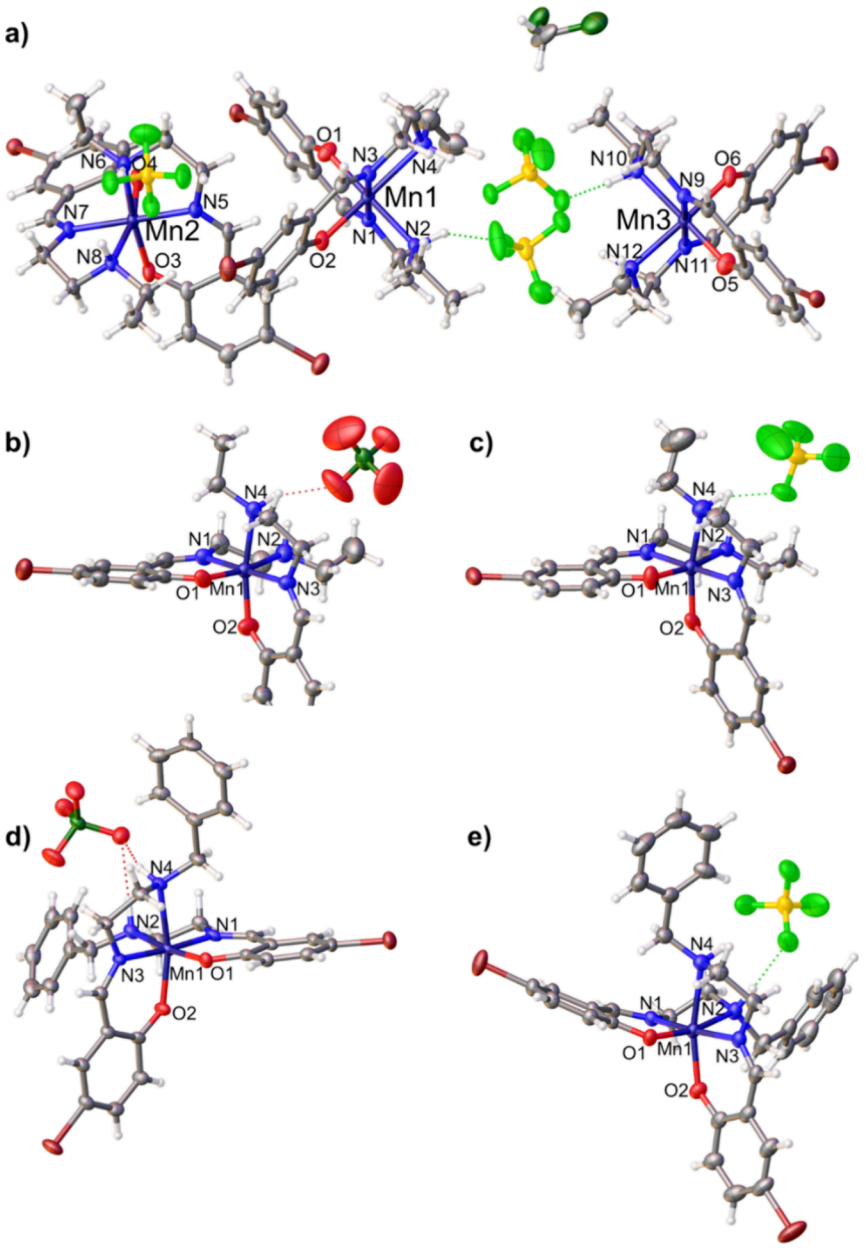

Figure 1. Asymmetric unit of (a) **2-dcm-hexane** at 100 K, (b) **1-hexane** at 150 K, (c) **2-dcm-hexane** at 150 K, (d) **3** at 150 K, and (d) **4** at 150 K (with 50% probability thermal ellipsoids). Color code: manganese, dark blue; N, blue; C, gray; O, red; F, green; Cl, dark green; Br, dark red; B, yellow; H, light gray.

consistent with the presence of a significant magnetic anisotropy and has been observed in other mononuclear Mn(III) SMMs.[38−45]

Considering this significant magnetic anisotropy for a single-spin $S_T = 2$, the experimental data of χT and M for **1**−**4** have been fitted successfully with an anisotropic Heisenberg Hamiltonian ($H = DS^2_{T,z} + E(S^2_{T,x} - S^2_{T,y})$) using the Phi software[77] to extract the experimental zero-field splitting parameters D and E, and g values (solid lines in Figure 3 and Figure S5). The best set of the obtained parameters are reported in Table 4. It is worth mentioning that alternative fits with a positive D value can be obtained but the E values are systematically above the rhombic value (1/3), while the experiment/theory agreement is slightly less good. Theoretical simulations from CASSCF and NEVPT2 calculations (dotted lines in Figure 3 and Figure S5) give good agreement with the experimental data. The CASSCF calculations lead to positive D value for **1** and **2** while negative values are obtained for **3** and **4**. In the case of **1**, the NEVPT2 calculations with ClO_4^- anions point toward a negative D value with a E value that is close to the rhombic limit as observed experimentally. In all the other cases, the CASSCF and NEVPT2 calculations lead to consistent results.

The dynamics of the magnetization has been probed in these complexes by alternating-current (ac) magnetic susceptibility measurements. For the $[Mn(salEen\text{-}Br)_2]^+$ cations (**1** and **2**), no out-of-phase signal, χ'', can be detected above 1.9 K, with frequencies up to 10,000 Hz and even with an external dc field up to 1 T. In contrast, the $[Mn(salBzen\text{-}Br)_2]^+$ cations (**3** and **4**) show a clear slow relaxation of the magnetization when applying a magnetic field (Figure 4 and Figure S6). For **3** and **4**, the out-of-phase signal is amplified in the presence of an external dc field

https://doi.org/10.1021/acs.inorgchem.4c01317
Inorg. Chem. 2024, 63, 12858−12869

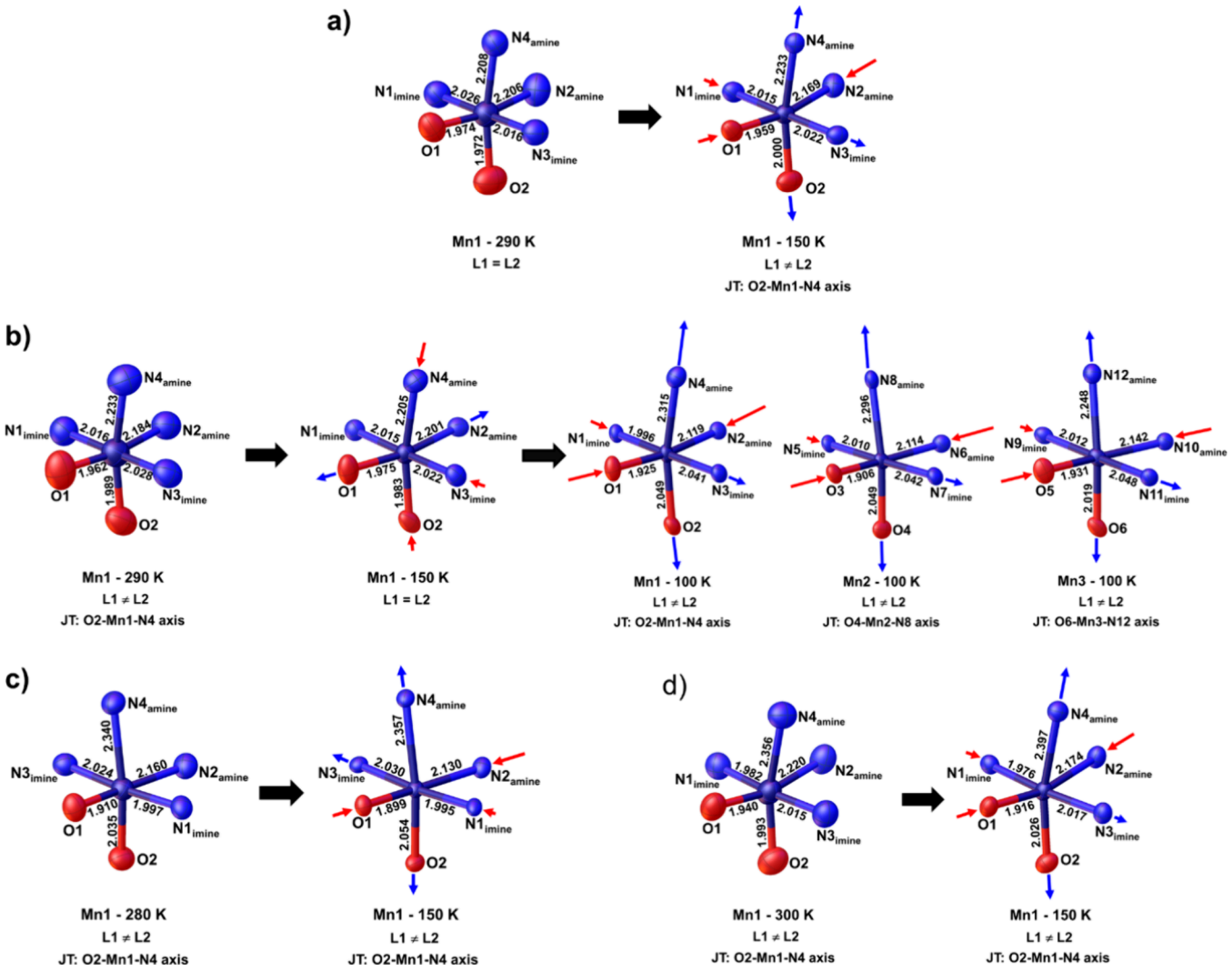

Figure 2. Coordination sphere of the Mn(III) complexes showing the changes in the Mn−N/O bond distances upon cooling for (a) **1-hexane**, (b) **2-dcm-hexane**, (c) **3**, and (d) **4** (with 50% probability thermal ellipsoids). Color code: manganese, dark blue; N, blue; O, red. The blue and red arrows represent elongation or compression of the Mn−N/O bonds, respectively, upon cooling with the size broadly indicative of the magnitude of the change. The bond distances and esd values of **1-hexane**, **2-dcm-hexane**, and **3**−**4** can be found in Table S2.

Table 2. Difference of Mn−N/O Bond Distances in Å between Ligands 1 and 2; L1 = Mn−O1, Mn−$N1_{imine}$, Mn−$N2_{amine}$ and L2 = Mn−O2, Mn−$N3_{imine}$, Mn−$N4_{amine}$ (esd Values in Parentheses)

	$[Mn(salEen\text{-}Br)_2]ClO_4$, 1-hexane		$[Mn(salEen\text{-}Br)_2]BF_4$, 2-dcm-hexane					$[Mn(salBzen\text{-}Br)_2]ClO_4$, **3**		$[Mn(salBzen\text{-}Br)_2]BF_4$, **4**	
					100 K						
bond list	290 K	150 K	290 K	150 K	**Mn1**	**Mn2**	**Mn3**	280 K	150 K	300 K	150 K
ΔMn−O[a]	−0.002(3)[d]	0.041(3)	0.027(5)	0.008(4)	0.124(3)	0.143(3)	0.088(3)	0.125(2)	0.155(2)	0.053(3)	0.110(2)
$\Delta Mn-N_{imine}$[b]	−0.010(3)[d]	0.007(3)	0.012(4)	0.007(3)	0.045(3)	0.032(3)	0.036(3)	0.027(3)	0.035(3)	0.033(3)	0.041(2)
$\Delta Mn-N_{amine}$[c]	0.002(3)	0.064(3)	0.049(4)	0.004(3)	0.196(4)	0.182(3)	0.106(3)	0.180(3)	0.227(3)	0.136(4)	0.223(3)
	L1 = L2	L1 ≠ L2	L1 ≠ L2	L1 = L2	L1 ≠ L2	L1 ≠ L2	L1 ≠ L2	L1 ≠ L2	L1 ≠ L2	L1 ≠ L2	L1 ≠ L2

[a]The bond distance of Mn1−O2 minus Mn1−O1, Mn2−O4 minus Mn2−O3, and Mn3−O6 minus Mn3−O5. [b]The bond distance of Mn1−$N3_{imine}$ minus Mn1−$N1_{imine}$, Mn2−$N7_{imine}$ minus Mn2−$N5_{imine}$, and Mn3−$N11_{imine}$ minus Mn3−$N9_{imine}$. [c]The bond distance of Mn1−$N4_{amine}$ minus Mn1−$N2_{amine}$, Mn2−$N8_{amine}$ minus Mn2−$N6_{amine}$, and Mn3−$N12_{amine}$ minus Mn3−$N10_{amine}$. [d]Negative values indicate that the L1 bond is longer than L2.

and shifted to lower frequency. At 2 K, a minimum of the characteristic frequency is observed for an optimized dc field of 0.3 and 0.4 T for **3** and **4**, respectively. Then, the temperature dependence of the relaxation has followed at these optimized fields. The full data sets (χ' vs ν and χ'' vs ν) at 2 K and the optimized field (Figure 4 and Figure S6) have been fitted to a generalized Debye model[78] to extract the corresponding relaxation time, τ, and to obtain their field and temperature evolutions (Figure 5 and Figure S7; note that the ESD of τ have been calculated with the log-normal distribution).[79,80] Finally, to analyze the paramagnetic relaxation mechanisms, the field and temperature dependence of τ has been fitted with eqs 1 and 2. It

https://doi.org/10.1021/acs.inorgchem.4c01317
Inorg. Chem. 2024, 63, 12858−12869

Table 3. Changing of the Bond Distances between Mn−N/O in Å; |ΔMn1−L| from High to Low Temperature (esd Values in Parentheses)

		[Mn(salEen-Br)$_2$]ClO$_4$, 1-hexane	[Mn(salEen-Br)$_2$]BF$_4$, 2-dcm-hexane				[Mn(salBzen-Br)$_2$]ClO$_4$, **3**	[Mn(salBzen-Br)$_2$]BF$_4$, **4**
				|ΔMn−L|$_{150-100K}$			
ligand	bond list	|ΔMn1−L|$_{290-150K}$	|ΔMn1−L|	|ΔMn2−L|[a]	|ΔMn3−L|[b]	|ΔMn1−L|$_{280-150K}$	|ΔMn1−L|$_{300-150K}$
L1	Mn1−O1	↓0.015(3)[c]	↑0.013(5)	↓0.050(4)	↓0.069(4)	↓0.044(4)	↓0.011(2)	↓0.024(2)
	Mn1−N1$_{imine}$	↓0.011(3)	↓0.001(4)	↓0.019(3)	↓0.005(3)	↓0.003(3)	↓0.002(3)	↓0.006(3)
	Mn1−N2$_{amine}$	↓0.037(3)	↑0.017(4)	↓0.082(3)	↓0.087(3)	↓0.059(3)	↓0.030(3)	↓0.046(3)
L2	Mn1−O2	↑0.028(3)[d]	↓0.006(3)	↑0.066(3)	↑0.066(3)	↑0.036(3)	↑0.019(2)	↑0.033(3)
	Mn1−N3$_{imine}$	↑0.006(3)	↓0.006(4)	↑0.019(3)	↑0.020(3)	↑0.026(3)	↑0.006(3)	↑0.002(3)
	Mn1−N4$_{amine}$	↑0.025(3)	↓0.028(4)	↑0.110(4)	↑0.091(3)	↑0.043(3)	↑0.017(2)	↑0.041(4)

[a]Mn2-L is Mn2-L1 = Mn2−O3, Mn2−N5$_{imine}$, Mn2−N6$_{amine}$ and Mn2-L2 = Mn2−O4, Mn2−N7$_{imine}$, Mn2−N8$_{amine}$. [b]Mn3-L is Mn3-L1 = Mn3−O5, Mn3−N9$_{imine}$, Mn3−N10$_{amine}$ and Mn3-L2 = Mn3−O6, Mn3−N11$_{imine}$, Mn3−N12$_{amine}$. [c]↓ = compressed Mn−N/O bond when decreasing temperature. [d]↑ = elongated Mn−N/O bond when decreasing temperature.

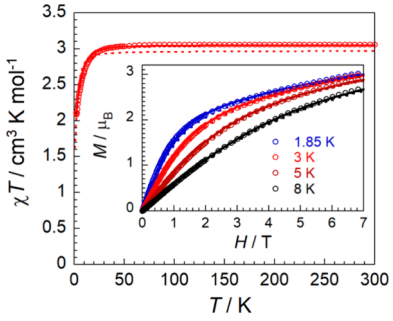

Figure 3. Temperature (T) dependence of the molar susceptibility (χ) at 1000 Oe shown as a χT versus T plot, and field dependence (H) of the magnetization M below 8 K (inset) for **1**. Open circles are experimental data, solid lines are best fits obtained from the Phi software[77] as discussed in the text, and dotted lines are theoretical χT versus T and M versus H plots calculated from theoretical approach. It should be noted that the fits and the calculated data are virtually superposed on the M versus H plot.

should be mentioned that the quantum tunneling of the magnetization process (QTM) has been omitted because there is no clear regime where this mechanism is dominant (i.e., no clear temperature independent regime).

$$\tau^{-1} = \tau_{Raman}^{-1} + \tau_{direct}^{-1} + \tau_{Orbach}^{-1} \quad (1)$$

$$\tau^{-1} = C\frac{1 + C_1H^2}{1 + C_2H^2}T^n + ATH^2 + \tau_0^{-1}\exp\left(\frac{-\Delta_{eff}}{k_BT}\right) \quad (2)$$

For complex **3**, the field dependence of the relaxation time (Figure 5) is small but the slow increase of the relaxation time below 0.3 T suggests a dominant Raman process and the slow decrease at a higher field indicates an additional direct process. The variation of the relaxation time in temperature (Figure 5) agrees with a dominant Raman process at low temperature (T^{-1} > 0.45 K^{-1}) and the presence of an additional thermally activated process (Arrhénius/Orbach-like) dominant at higher temperature (T^{-1} < 0.36 K^{-1}). The full data set for **3** can be described accurately (Figure 5) with the parameters C = 960 K^{-n} s^{-1}, C_1 = 23 T^{-2}, C_2 = 110 T^{-2}, n = 3.7, and A = 6000 T^{-4} K^{-1} s^{-1} and τ_0 = 1.8 × 10^{-9} s, Δ_{eff}/k_B = 27.9 K for Raman, direct, and Orbach relaxation mechanisms, respectively.

In the case of **4**, the behavior is similar but the relaxation time is slightly shorter in the same temperature, dc field, and ac frequency windows (Figure S6). The field dependence of the relaxation is small with a slow increase of the relaxation time below 0.2 T, suggesting a contribution of a Raman process, while the effect of a Direct process is negligible at higher fields (Figure S7). On the other hand, the variation of the relaxation time in temperature (Figure S7) suggests a dominant thermally activated relaxation (Arrhénius/Orbach-like). Considering the value of the parameters extracted from the sole fitting of the temperature dependence by an Orbach-like process, this mechanism is dominant in the field dependence for the field above 0.1 T, reducing the contribution of the Raman process. The full relaxation time data set (field and temperature dependences) can be described accurately with the parameters C = 2800 K^{-n} s^{-1}, C_1 = 23 T^{-2}, C_2 = 520 T^{-2}, n = 3.7, τ_0 = 1.8 × 10^{-9} s, and Δ_{eff}/k_B = 20.7 K for Raman and Orbach-like relaxation mechanisms, respectively.

The experimental energy gaps of the Orbach process in **3** and **4** (27.9 and 20.7 K, respectively) agree relatively well with the energy splitting ($\Delta = DS_T^2$; 28 or 24 K for **3** and **4**, respectively)

Table 4. Zero-Field Splitting Parameters D and E in K, and g Values (esd Values in Parentheses) Obtained from the Fitting of the Experimental Magnetic Data as well as the Calculated CASSCF and NEVPT2 Values of D and E in K for 1−4

complex		SMM	g	D, E	D_{CASSCF}, $\|E_{CASSCF}\|$	D_{NEVPT2}, $\|E_{NEVPT2}\|$
[Mn(salEen-Br)$_2$]ClO$_4$	**1**	no	2.01(5)	−7.5, 1.8	4.8, 1.4	−7.0, 2.3
[Mn(salEen-Br)$_2$]$^+$ without ClO$_4^-$	**1**$^+$				5.0, 1.2	7.2, 1.8
[Mn(salEen-Br)$_2$]BF$_4$	**2**	no	1.99(5)	−7.7, 2.4	5.50, 0.13	8.20, 0.09
[Mn(salEen-Br)$_2$]$^+$ without BF$_4^-$	**2**$^+$				5.44, 0.22	7.91, 0.28
[Mn(salBzen-Br)$_2$]ClO$_4$	**3**	yes	1.99(5)	−7.0, 2.3	−5.01, 0.27	−6.72, 0.33
[Mn(salBzen-Br)$_2$]$^+$ without ClO$_4^-$	**3**$^+$				−4.94, 0.40	−6.47, 0.43
[Mn(salBzen-Br)$_2$]BF$_4$	**4**	yes	1.99(5)	−6.0, 1.5	−4.73, 0.91	−6.17, 0.92
[Mn(salBzen-Br)$_2$]$^+$ without BF$_4^-$	**4**$^+$				−4.6, 1.0	−6.0, 1.1

https://doi.org/10.1021/acs.inorgchem.4c01317
Inorg. Chem. 2024, 63, 12858−12869

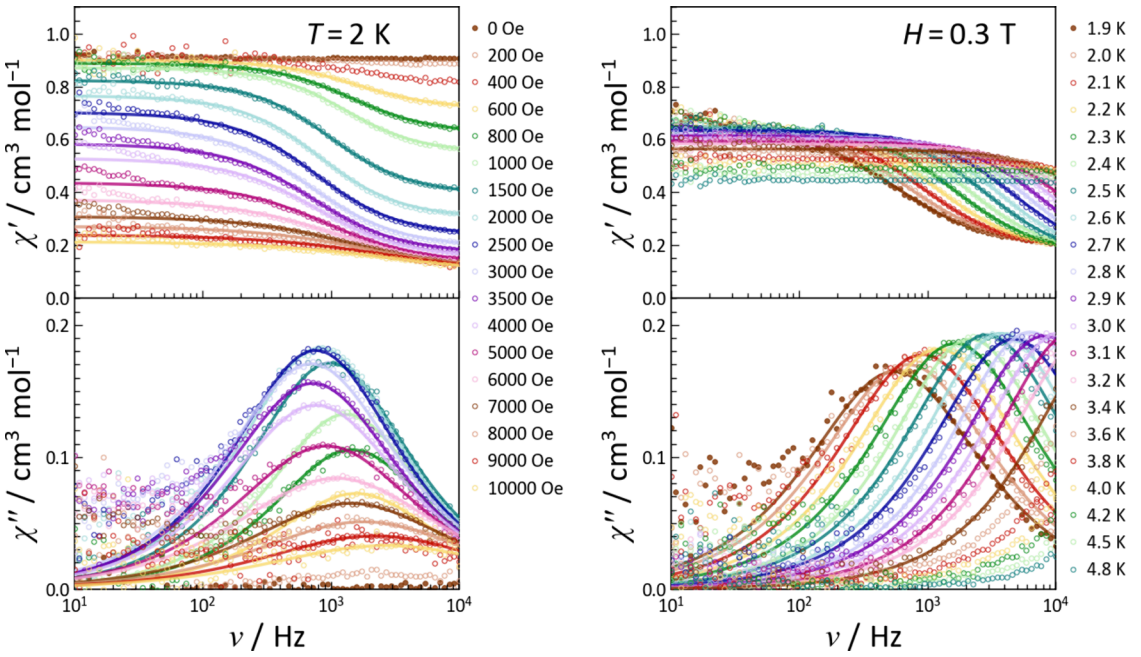

Figure 4. Frequency dependence of the in-phase (top; χ') and out-of-phase (bottom; χ'') components of the ac susceptibility at 2 K and indicated dc field between 0 and 1 T (left) and at 0.3 T and indicated temperatures between 1.9 and 4.8 K for **3**. Solid lines are best fits to the generalized Debye model.

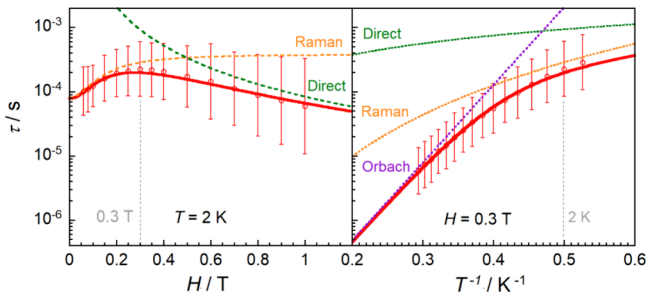

Figure 5. Left: field dependence of the relaxation time (plotted as τ vs H in the semilogarithm scale) at 2 K for **3**. Right: temperature dependence of the relaxation time (plotted as τ vs T^{-1} in the semilogarithm scale) at 0.3 T for **3**. Open circles are the experimental data, and bars denote ESDs of distribution of times from the generalized Debye model. Solid lines are the result of the best global simulation, as discussed in the text. Dotted lines are Raman (orange), direct (green), and Orbach (purple) components of the model.

induced by the zero-field splitting (D) on the $S = 2$ ground state. The results reveal relatively minor differences between the two complexes, indicating that the anion has only a small impact on the paramagnetic relaxation time in **3** and **4**. In contrast, the magnetic studies clearly reveal that the benzyl group on the salBzen-Br ligand is important for observing the SMM properties. Compared to other mononuclear Mn(III) systems, the Δ_{eff} of these new complexes is significantly higher (Table S3).[38−45]

Electronic Structure Calculations. To better understand the magnetic properties of $\mathbf{1}^{+}$−$\mathbf{4}^{+}$, *ab initio* calculations were undertaken. In order to detect the SMM behavior in the Mn complex, it is necessary to have a uniaxial magnetic anisotropy and thus a negative D value. The spin−orbit operator connecting the ground and excited states plays a crucial role in determining the sign and value of the D parameter. Negative D values can result from the first excitation of orbitals with identical $|m_l|$ values, d_{xz} and d_{yz} ($m_l = \pm 1$) or d_{xy} and $d_{x^2-y^2}$ ($m_l = \pm 2$), while excitation between orbitals where $|\Delta m_l| = 1$ results in a positive D value.[81] As noted in Table 4, experimental negative D values are observed for all the complexes, and alternative fits with a positive D value lead to E values systematically above the rhombic value (1/3) and a lower experiment/theory agreement. The R group on the salRen-Br ligand (R = ethyl or benzyl group) clearly influences the molecular orientation. The large D contribution of $[Mn(salEen\text{-}Br)_2]^+$ in multiplicity = 5 comes from the first excitation from d_{yz} to d_{z^2} ($|\Delta m_l| = 1$), leading to a calculated positive D value as shown Figure S8. In contrast, the negative D values in $[Mn(salBzen\text{-}Br)_2]^+$ are caused by the excitation from d_{xy} to $d_{x^2-y^2}$ (the same $|m_l|$), as illustrated in Figure S9.

The energies of the d orbitals computed using the *ab initio* ligand field theory (AILFT)[70,82] approach are shown in Figure 6 and Table S4. As expected, the degeneracy of the d orbitals is

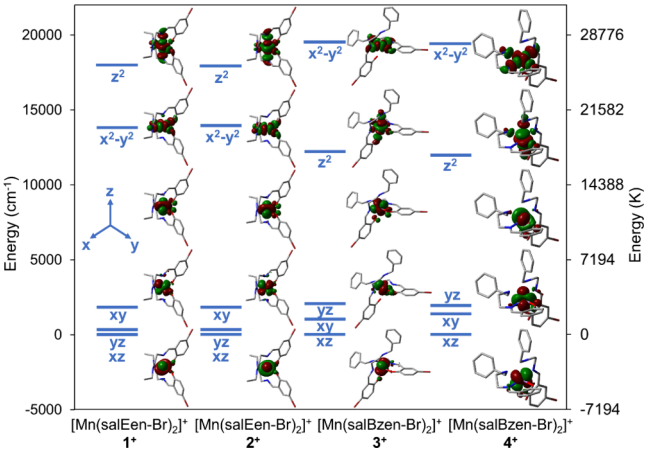

Figure 6. Calculated AILFT d orbital energies using the NEVPT2 method.

https://doi.org/10.1021/acs.inorgchem.4c01317
Inorg. Chem. 2024, 63, 12858−12869

broken due to the Jahn−Teller distortion of the Mn(III) centers observed in the structural studies at 150 K (or 100 K in the case of **2**). For the $[Mn(salEen\text{-}Br)_2]^+$ complexes, the d_{xy} orbital is clearly separated from d_{xz} and d_{yz} by *ca.* 1500 cm^{-1}, while the d_{z^2} orbital is highest in energy, *ca.* 4500 cm^{-1} above the $d_{x^2-y^2}$ orbital. Interestingly for the $[Mn(salBzen\text{-}Br)_2]^+$ cations, the formally t_{2g} set of orbitals are distributed such that the d_{xy} orbital is closer in energy to that of d_{yz}. It is also noteworthy that the $d_{x^2-y^2}$ and d_{z^2} orbitals are much further apart in the case of $\mathbf{3}^+$ and $\mathbf{4}^+$ than in $\mathbf{1}^+$ and $\mathbf{2}^+$ and may suggest that a greater degree of orbital mixing is permitted, which could explain the difficulties in observing the Jahn−Teller axes at higher temperature in the structural studies of the $[Mn(salEen\text{-}Br)_2]^+$ series. Similar observations have been made in $[Mn(F\text{-}salk_2\text{-}323)]$ {F-salk$_2$-323 = *N*,*N*′-bis(3-(2-(2-oxy-4-fluorobenzyl)methylideneamino)propyl)-ethylenediamine} where larger anions result in reorientation of the Jahn−Teller axis.[83]

CONCLUSIONS

In summary, four new $[Mn(salRen\text{-}Br)_2]Y$ (Y = ClO_4^- and BF_4^-) complexes have been prepared to study the effect of the substituent R and the Y anion. Thermal effects on the Jahn−Teller distortion at the Mn(III) center are limited principally to the salEen-Br complexes. The axially elongated axis is ambiguous at high temperature, whereas it becomes obvious low temperature. For **1**, **3**, and **4**, a clear Jahn−Teller distortion is observed at 150 K but it is not the case for **2**. Indeed, this complex shows a phase transition with a symmetry breaking between the monoclinic $P2_1/c$ space group at 150 K and the monoclinic $P2_1/n$ space group at 100 K. At this temperature, a strong Jahn−Teller distortion is observed at the Mn(III) centers in **2**. The study of the static and dynamics magnetic properties of these complexes revealed that the benzyl group on the salBzen-Br ligand is essential for observing the SMM properties perhaps due to the more pronounced Jahn−Teller distortion in these systems, while the ClO_4^- and BF_4^- anions have a subtler impact on the Orbach energy barrier. Theoretical studies suggest that complexes **1** and **2** reveal positive *D* values while **3** and **4** exhibit negative *D* values, and this is the principal reason for the observation of SMM behavior in these systems. In contrast, magnetic studies suggest negative *D* values for all complexes. Further work with a wider variety of alkyl groups, substituents, and anions is currently underway to better understand this contradiction.

ASSOCIATED CONTENT

Supporting Information

The Supporting Information is available free of charge at https://pubs.acs.org/doi/10.1021/acs.inorgchem.4c01317.

IR and UV−vis spectra, TGA curve, Mn−N/O bond distances, Cole−Cole and Arrhenius plots, and magnetic parameters for the reported mononuclear Mn(III) SMMs (PDF)

Accession Codes

CCDC 2344242−2344250 contain the supplementary crystallographic data for this paper. These data can be obtained free of charge via www.ccdc.cam.ac.uk/data_request/cif or by emailing data_request@ccdc.cam.ac.uk or by contacting The Cambridge Crystallographic Data Centre, 12 Union Road, Cambridge CB2 1EZ, UK; fax: + 441223336033

AUTHOR INFORMATION

Corresponding Authors

Phimphaka Harding − *School of Chemistry, Institute of Science, Suranaree University of Technology, Nakhon Ratchasima 30000, Thailand;* orcid.org/0000-0002-7253-316X; Email: phimphaka@g.sut.ac.th

David J. Harding − *School of Chemistry, Institute of Science, Suranaree University of Technology, Nakhon Ratchasima 30000, Thailand;* orcid.org/0000-0001-8866-2401; Email: david@g.sut.ac.th

Authors

Chantalaksana Chantarangkul − *Functional Materials and Nanotechnology Centre of Excellence, Walailak University, Nakhon Si Thammarat 80160, Thailand*

Apinya Patigo − *Functional Materials and Nanotechnology Centre of Excellence, Walailak University, Nakhon Si Thammarat 80160, Thailand*

John C. McMurtrie − *Queensland University of Technology (QUT), Brisbane, Queensland 4001, Australia;* orcid.org/0000-0003-3990-8617

Rodolphe Clérac − *University of Bordeaux, CNRS, CRPP, UMR 5031, F-33600 Pessac, France;* orcid.org/0000-0001-5429-7418

Mathieu Rouzières − *University of Bordeaux, CNRS, CRPP, UMR 5031, F-33600 Pessac, France*

Silvia Gómez-Coca − *Departament de Química Inorgànica i Orgànica, Institut de Recerca de Química Teòrica i Computacional, Universitat de Barcelona, 08028 Barcelona, Spain*

Eliseo Ruiz − *Departament de Química Inorgànica i Orgànica, Institut de Recerca de Química Teòrica i Computacional, Universitat de Barcelona, 08028 Barcelona, Spain*

Complete contact information is available at: https://pubs.acs.org/10.1021/acs.inorgchem.4c01317

Author Contributions

C.C.: investigation, formal analysis, data curation, visualization, writing—original draft. A.P.: investigation, data curation. J.C.M.: investigation, data curation. R.C.: investigation, formal analysis, data curation, writing—review and editing. M.R.: investigation, formal analysis, data curation, review and editing. S.G.-C.: investigation, formal analysis, data curation. E.R.: methodology, investigation, formal analysis, data curation, resources, writing—review and editing, funding acquisition. P.H.: conceptualization, resources, writing—review and editing, supervision. D.J.H.: conceptualization, resources, writing—review and editing, supervision, funding acquisition.

Notes

The authors declare no competing financial interest.

ACKNOWLEDGMENTS

This research has received funding support from the NSRF *via* the Program Management Unit for Human Resources & Institutional Development, Research and Innovation (grant number: B39G670018). We gratefully acknowledge Suranaree University of Technology for partial financial support through the Molecular Magnetic Materials Research Unit. Walailak University is thanked for support from the Functional Materials and Nanotechnology Centre of Excellence, Walailak University, Thailand. Special gratitude goes to the Development and Promotion of Science and Technology Talents Project (DPST)

(grant number: WU602118-1/60) and the Walailak University Graduate Research Fund (contract no. CGS-RF-2022/10) for scholarships to C.C. R.C. and M.R. thank the University of Bordeaux, the Région Nouvelle Aquitaine, Quantum Matter Bordeaux (QMBx), the Centre National de la Recherche Scientifique (CNRS), and the Association Française de Magnétisme Moléculaire as well as the financial support from Ministerio de Ciencia, Innovación y Universidades (PID2021-122464NB-I00, TED2021-129593B-I00, and Maria de Maeztu CEX2021-001202-M). We also acknowledge the Generalitat de Catalunya for the 2021-SGR-00286 grant and E.R. for an ICREA Academia grant. We are grateful for the computational resources provided by the CSUC supercomputer center.

REFERENCES

(1) Ripka, P.; Arafat, M. M. Magnetic Sensors: Principles and Applications. *Ref. Modul. Mater. Sci. Mater. Eng.* **2019**, *1* (March), 1−15.
(2) Sessoli, R.; Gatteschi, D.; Caneschi, A.; Novak, M. A. Magnetic Bistability in a Metal-Ion Cluster. *Nature* **1993**, *365* (6442), 141−143.
(3) Gatteschi, D.; Sessoli, R.; Villain, J. *Molecular nanomagnets*; Oxford University Press, 2006. DOI: 10.1093/acprof:oso/9780198567530.001.0001.
(4) Frost, J. M.; Harriman, K. L. M.; Murugesu, M. The Rise of 3-d Single-Ion Magnets in Molecular Magnetism: Towards Materials from Molecules? *Chem. Sci.* **2016**, *7* (4), 2470−2491.
(5) Sessoli, R.; Gatteschi, D.; Tsai, H. L.; Hendrickson, D. N.; Schake, A. R.; Wang, S.; Vincent, J. B.; Christou, G.; Folting, K. High-Spin Molecules: $[Mn_{12}O_{12}(O_2CR)_{16}(H_2O)_4]$. *J. Am. Chem. Soc.* **1993**, *115* (5), 1804−1816.
(6) Murugesu, M.; Habrych, M.; Wernsdorfer, W.; Abboud, K. A.; Christou, G. Single-Molecule Magnets: A Mn_{25} Complex with a Record S = 51/2 Spin for a Molecular Species. *J. Am. Chem. Soc.* **2004**, *126*, 4766−4767.
(7) Stamatatos, T. C.; Abboud, K. A.; Wernsdorfer, W.; Christou, G. Covalently Linked Dimers of Clusters: Loop- and Dumbbell-Shaped Mn_{24} and Mn_{26} Single-Molecule Magnets. *Angew. Chem., Int. Ed.* **2008**, *47*, 6694−6698.
(8) Thuijs, A. E.; King, P.; Abboud, K. A.; Christou, G. New Structural Types of Mn_{16} Single-Molecule Magnets: W-Shaped Topology from Reductive Aggregation. *Inorg. Chem.* **2015**, *54*, 9127−9137.
(9) Abbasi, P.; Quinn, K.; Alexandropoulos, D. I.; Damjanovic, M.; Wernsdorfer, W.; Escuer, A.; Mayans, J.; Pilkington, M.; Stamatatos, T. C. Transition Metal Single-Molecule Magnets: A $\{Mn_{31}\}$ Nanosized Cluster with a Large Energy Barrier of ∼ 60 K and Magnetic Hysteresis at ∼ 5 K. *J. Am. Chem. Soc.* **2017**, *139*, 15644−15647.
(10) Shiga, T.; Nojiri, H.; Oshio, H. A Ferromagnetically Coupled Octanuclear Manganese(III) Cluster: A Single-Molecule Magnet with a Spin Ground State of S = 16. *Inorg. Chem.* **2020**, *59*, 4163−4166.
(11) Milios, C. J.; Vinslava, A.; Wernsdorfer, W.; Moggach, S.; Parsons, S.; Perlepes, S. P.; Christou, G.; Brechin, E. K. A Record Anisotropy Barrier for a Single-Molecule Magnet. *J. Am. Chem. Soc.* **2007**, *129*, 2754−2755.
(12) Blake, A. J.; Grant, C. M.; Parsons, S.; Rawson, J. M.; Winpenny, R. E. P. The Synthesis, Structure and Magnetic Properties of a Cyclic Dodecanuclear Nickel Complex. *J. Chem. Soc. Chem. Commun.* **1994**, 2363−2364.
(13) Castro, S. L.; Sun, Z.; Bollinger, J. C.; Hendrickson, D. N.; Christou, G. Tetranuclear Vanadium(III) Carboxylate Chemistry, and a New Example of a Metal Butterfly Complex Exhibiting Spin Frustration: Structure and Properties of $[V_4O_2(O_2CEt)_7(Bpy)_2]$-$(ClO_4)$. *J. Chem. Soc. Chem. Commun.* **1995**, *24*, 2517−2518.
(14) Langley, S. K.; Chilton, N. F.; Moubaraki, B.; Murray, K. S. Anisotropy Barrier Enhancement via Ligand Substitution in Tetranuclear $\{Co^{III}_2Ln^{III}_2\}$ Single Molecule Magnets. *Chem. Commun.* **2013**, *49* (62), 6965−6967.
(15) Liu, J.-L.; Chen, Y.-C.; Zheng, Y.-Z.; Lin, W.-Q.; Ungur, L.; Wernsdorfer, W.; Chibotaru, L. F.; Tong, M.-L. Switching the Anisotropy Barrier of a Single-Ion Magnet by Symmetry Change from Quasi-D_{5h} to Quasi-Oh. *Chem. Sci.* **2013**, *4* (8), 3310−3316.
(16) Langley, S. K.; Le, C.; Ungur, L.; Moubaraki, B.; Abrahams, B. F.; Chibotaru, L. F.; Murray, K. S. Heterometallic 3d−4f Single-Molecule Magnets: Ligand and Metal Ion Influences on the Magnetic Relaxation. *Inorg. Chem.* **2015**, *54* (7), 3631−3642.
(17) Sun, W.-B.; Yan, P.-F.; Jiang, S.-D.; Wang, B.-W.; Zhang, Y.-Q.; Li, H.-F.; Chen, P.; Wang, Z.-M.; Gao, S. High Symmetry or Low Symmetry, That Is the Question − High Performance Dy(III) Single-Ion Magnets by Electrostatic Potential Design. *Chem. Sci.* **2016**, *7* (1), 684−691.
(18) Amjad, A.; Madalan, A. M.; Andruh, M.; Caneschi, A.; Sorace, L. Slow Relaxation of Magnetization in an Isostructural Series of Zinc−Lanthanide Complexes: An Integrated EPR and AC Susceptibility Study. *Chem. − Eur. J.* **2016**, *22* (36), 12849−12858.
(19) Lin, P. H.; Tsui, E. Y.; Habib, F.; Murugesu, M.; Agapie, T. Effect of the Mn Oxidation State on Single-Molecule-Magnet Properties: Mn^{III} vs Mn^{IV} in Biologically Inspired $DyMn_3O_4$ Cubanes. *Inorg. Chem.* **2016**, *55* (12), 6095−6099.
(20) Zhou, G. J.; Han, T.; Ding, Y. S.; Chilton, N. F.; Zheng, Y. Z. Metallacrowns as Templates for Diabolo-like $\{LnCu_8\}$ Complexes with Nearly Perfect Square Antiprismatic Geometry. *Chem. - A Eur. J.* **2017**, *23* (62), 15617−15622.
(21) Li, J.; Wei, R. M.; Pu, T. C.; Cao, F.; Yang, L.; Han, Y.; Zhang, Y. Q.; Zuo, J. L.; Song, Y. Tuning Quantum Tunnelling of Magnetization through 3d-4f Magnetic Interactions: An Alternative Approach for Manipulating Single-Molecule Magnetism. *Inorg. Chem. Front.* **2017**, *4* (1), 114−122.
(22) Wang, H. S.; Zhang, K.; Song, Y.; Pan, Z. Q. Recent Advances in 3d-4f Magnetic Complexes with Several Types of Non-Carboxylate Organic Ligands. *Inorg. Chim. Acta* **2021**, *521* (August 2020), No. 120318.
(23) Barra, A.-L.; Debrunner, P.; Gatteschi, D.; Schulz, C. E.; Sessoli, R. Superparamagnetic-like Behavior in an Octanuclear Iron Cluster. *Europhys. Lett.* **1996**, *35*, 133−138.
(24) Parsons, S.; Solan, G. A.; Winpenny, R. E. P.; Benelli, C. Ferric Wheels and Cages: Decanuclear Iron Complexes with Carboxylato and Pyridonato Ligands. *Angew. Chem., Int. Ed.* **1996**, *16*, 1825−1828.
(25) Brechin, E. K.; Soler, M.; Davidson, J.; Hendrickson, D. N.; Parsons, S.; Christou, G. A New Class of Single-Molecule Magnet: $[Mn_9O_7(OAc)_{11}(thme)(py)_3(H_2O)_2]$ with an S = 17/2 Ground State. *Chem. Commun.* **2002**, *19*, 2252−2253.
(26) Bell, A.; Aromı, G.; Teat, S. J.; Wernsdorfer, W.; Winpenny, R. E. P. Synthesis and Characterisation of a $\{Ni_8\}$ Single Molecule Magnet and Another Octanuclear Nickel Cage. *Chem. Commun.* **2005**, 2808−2810.
(27) Aromí, G.; Brechin, E. K.; Winpenny, R. Synthesis of 3d Metallic Single-Molecule Magnets. *Struct. Bonding* **2006**, *122* (January), 1−67.
(28) Li, X. L.; Min, F. Y.; Wang, C.; Lin, S. Y.; Liu, Z.; Tang, J. $[Ln^{III}$−Mn^{II}−$Ln^{III}]$ Heterometallic Compounds: Rare Linear SMMs with Divalent Manganese Ions. *Dalton Trans.* **2015**, *44*, 3430−3438.
(29) Modak, R.; Sikdar, Y.; Cosquer, G.; Chatterjee, S.; Yamashita, M.; Goswami, S. Heterometallic Cu^{II}-Dy^{III} Clusters of Different Nuclearities with Slow Magnetic Relaxation. *Inorg. Chem.* **2016**, *55* (2), 691−699.
(30) Hołyńska, M.; Premužić, D.; Jeon, I.; Wernsdorfer, W.; Clérac, R.; Dehnen, S. $[Mn^{III}_6O_3Ln_2]$ Single-Molecule Magnets: Increasing the Energy Barrier Above 100 K. *Chem. − Eur. J.* **2011**, *17* (35), 9605−9610.
(31) Liu, J. L.; Wu, J. Y.; Chen, Y. C.; Mereacre, V.; Powell, A. K.; Ungur, L.; Chibotaru, L. F.; Chen, X. M.; Tong, M. L. A Heterometallic Fe^{II}-Dy^{III} Single-Molecule Magnet with a Record Anisotropy Barrier. *Angew. Chem., Int. Ed.* **2014**, *53* (47), 12966−12970.
(32) Liu, J.-L.; Wu, J.-Y.; Huang, G.-Z.; Chen, Y.-C.; Jia, J.-H.; Ungur, L.; Chibotaru, L. F.; Chen, X.-M.; Tong, M.-L. Desolvation-Driven 100-Fold Slow-down of Tunneling Relaxation Rate in Co(II)-Dy(III) Single-Molecule Magnets through a Single-Crystal-to-Single-Crystal Process. *Sci. Rep.* **2015**, *5* (1), 16621.

(33) Ishikawa, N.; Sugita, M.; Ishikawa, T.; Koshihara, S. Y.; Kaizu, Y. Lanthanide Double-Decker Complexes Functioning as Magnets at the Single-Molecular Level. *J. Am. Chem. Soc.* **2003**, *125* (29), 8694−8695.
(34) Goodwin, C. A. P.; Ortu, F.; Reta, D.; Chilton, N. F.; Mills, D. P. Molecular Magnetic Hysteresis at 60 K in Dysprosocenium. *Nature* **2017**, *548* (7668), 439−442.
(35) Samuel, P. P.; Mondal, K. C.; Amin Sk, N.; Roesky, H. W.; Carl, E.; Neufeld, R.; Stalke, D.; Demeshko, S.; Meyer, F.; Ungur, L.; Chibotaru, L. F.; Christian, J.; Ramachandran, V.; Van Tol, J.; Dalal, N. S. Electronic Structure and Slow Magnetic Relaxation of Low-Coordinate Cyclic Alkyl(amino) Carbene Stabilized Iron(I) Complexes. *J. Am. Chem. Soc.* **2014**, *136* (34), 11964−11971.
(36) Feng, X.; Mathonière, C.; Jeon, I. R.; Rouzières, M.; Ozarowski, A.; Aubrey, M. L.; Gonzalez, M. I.; Clérac, R.; Long, J. R. Tristability in a Light-Actuated Single-Molecule Magnet. *J. Am. Chem. Soc.* **2013**, *135* (42), 15880−15884.
(37) Mossin, S.; Tran, B. L.; Adhikari, D.; Pink, M.; Heinemann, F. W.; Sutter, J.; Szilagyi, R. K.; Meyer, K.; Mindiola, D. J. A Mononuclear Fe(III) Single Molecule Magnet with a 3/2↔5/2 Spin Crossover. *J. Am. Chem. Soc.* **2012**, *134* (33), 13651−13661.
(38) Vallejo, J.; Pascual-Álvarez, A.; Cano, J.; Castro, I.; Julve, M.; Lloret, F.; Krzystek, J.; De Munno, G.; Armentano, D.; Wernsdorfer, W.; Ruiz-García, R.; Pardo, E. Field-Induced Hysteresis and Quantum Tunneling of the Magnetization in a Mononuclear Manganese(III) Complex. *Angew. Chem., Int. Ed.* **2013**, *52* (52), 14075−14079.
(39) Ishikawa, R.; Miyamoto, R.; Nojiri, H.; Breedlove, B. K.; Yamashita, M. Slow Relaxation of the Magnetization of an Mn^{III} Single Ion. *Inorg. Chem.* **2013**, *52* (15), 8300−8302.
(40) Grigoropoulos, A.; Pissas, M.; Papatolis, P.; Psycharis, V.; Kyritsis, P.; Sanakis, Y. Spin-Relaxation Properties of a High-Spin Mononuclear $Mn^{III}O_6$-Containing Complex. *Inorg. Chem.* **2013**, *52* (22), 12869−12871.
(41) Chen, L.; Wang, J.; Liu, Y. Z.; Song, Y.; Chen, X. T.; Zhang, Y. Q.; Xue, Z. L. Slow Magnetic Relaxation in Mononuclear Octahedral Manganese(III) Complexes with Dibenzoylmethanide Ligands. *Eur. J. Inorg. Chem.* **2015**, *2015* (2), 271−278.
(42) Craig, G. A.; Marbey, J. J.; Hill, S.; Roubeau, O.; Parsons, S.; Murrie, M. Field-Induced Slow Relaxation in a Monometallic Manganese(III) Single-Molecule Magnet. *Inorg. Chem.* **2015**, *54* (1), 13−15.
(43) Pascual-Álvarez, A.; Vallejo, J.; Pardo, E.; Julve, M.; Lloret, F.; Krzystek, J.; Armentano, D.; Wernsdorfer, W.; Cano, J. Field-Induced Slow Magnetic Relaxation in a Mononuclear Manganese(III)-Porphyrin Complex. *Chem. - A Eur. J.* **2015**, *21* (48), 17299−17307.
(44) Liu, Y. M.; Liu, Z. Y.; Yang, E. C.; Zhao, X. J. Field-Induced Slow Relaxation of a Manganese(III)-Based Single-Ion Magnet. *Inorg. Chem. Commun.* **2017**, *77*, 27−30.
(45) Realista, S.; Fitzpatrick, A. J.; Santos, G.; Ferreira, L. P.; Barroso, S.; Pereira, L. C. J.; Bandeira, N. A. G.; Neugebauer, P.; Hrubý, J.; Morgan, G. G.; Van Slageren, J.; Calhorda, M. J.; Martinho, P. N. A Mn(III) Single Ion Magnet with tridentate Schiff-Base Ligands. *Dalton Trans.* **2016**, *45* (31), 12301−12307.
(46) Zadrozny, J. M.; Long, J. R. Slow Magnetic Relaxation at Zero Field in the Tetrahedral Complex $[Co(SPh)_4]^{2-}$. *J. Am. Chem. Soc.* **2011**, *133* (51), 20732−20734.
(47) Habib, F.; Luca, O. R.; Vieru, V.; Shiddiq, M.; Korobkov, I.; Gorelsky, S. I.; Takase, M. K.; Chibotaru, L. F.; Hill, S.; Crabtree, R. H.; Murugesu, M. Influence of the Ligand Field on Slow Magnetization Relaxation versus Spin Crossover in Mononuclear Cobalt Complexes. *Angew. Chem., Int. Ed.* **2013**, *52* (43), 11290−11293.
(48) Eichhöfer, A.; Lan, Y.; Mereacre, V.; Bodenstein, T.; Weigend, F. Slow Magnetic Relaxation in Trigonal-Planar Mononuclear Fe(II) and Co(II) Bis(trimethylsilyl)amido Complexes - A Comparative Study. *Inorg. Chem.* **2014**, *53* (4), 1962−1974.
(49) Novikov, V. V.; Pavlov, A. A.; Nelyubina, Y. V.; Boulon, M. E.; Varzatskii, O. A.; Voloshin, Y. Z.; Winpenny, R. E. P. A Trigonal Prismatic Mononuclear Cobalt(II) Complex Showing Single-Molecule Magnet Behavior. *J. Am. Chem. Soc.* **2015**, *137* (31), 9792−9795.
(50) Poulten, R. C.; Page, M. J.; Algarra, A. G.; Le Roy, J. J.; López, I.; Carter, E.; Llobet, A.; Macgregor, S. A.; Mahon, M. F.; Murphy, D. M.; Murugesu, M.; Whittlesey, M. K. Synthesis, Electronic Structure, and Magnetism of $[Ni(6\text{-}Mes)_2]^+$: A Two-Coordinate Nickel(I) Complex Stabilized by Bulky N-Heterocyclic Carbenes. *J. Am. Chem. Soc.* **2013**, *135* (37), 13640−13643.
(51) Miklovič, J.; Valigura, D.; Boča, R.; Titiš, J. Mononuclear Ni(II) Complex: A Field Induced Single-Molecule Magnet Showing Two Slow Relaxation Processes. *Dalton Trans.* **2015**, *44*, 12484.
(52) Marriott, K. E. R.; Bhaskaran, L.; Wilson, C.; Medarde, M.; Ochsenbein, S. T.; Hill, S.; Murrie, M. Pushing the Limits of Magnetic Anisotropy in Trigonal Bipyramidal Ni(II). *Chem. Sci.* **2015**, *6* (12), 6823−6828.
(53) Deng, Y. F.; Han, T.; Wang, Z.; Ouyang, Z.; Yin, B.; Zheng, Z.; Krzystek, J.; Zheng, Y. Z. uniaxial Magnetic Anisotropy of Square-Planar Chromium(II) Complexes Revealed by Magnetic and HF-EPR Studies. *Chem. Commun.* **2015**, *51* (100), 17688−17691.
(54) Cirera, J.; Ruiz, E.; Alvarez, S.; Neese, F.; Kortus, J. How to Build Molecules with Large Magnetic Anisotropy. *Chem. - A Eur. J.* **2009**, *15* (16), 4078−4087.
(55) Cardoso, B. D. P.; Vicente, A. I.; Ward, J. B. J.; Sebastião, P. J.; Chávez, F. V.; Barroso, S.; Carvalho, A.; Keely, S. J.; Martinho, P. N.; Calhorda, M. J. Fe(III) SalEen Derived Schiff Base Complexes as Potential Contrast Agents. *Inorg. Chim. Acta* **2015**, *432*, 258−266.
(56) Vicente, A. I.; Joseph, A.; Ferreira, L. P.; De Deus Carvalho, M.; Rodrigues, V. H. N.; Duttine, M.; Diogo, H. P.; Minas Da Piedade, M. E.; Calhorda, M. J.; Martinho, P. N. Dynamic Spin Interchange in a tridentate Fe(III) Schiff-Base Compound. *Chem. Sci.* **2016**, *7* (7), 4251−4258.
(57) Al-Azzani, M. A.; Al-Mjeni, F.; Mitsuhashi, R.; Mikuriya, M.; Al-Omari, I. A.; Robertson, C. C.; Bill, E.; Shongwe, M. S. Unusual Magneto-Structural Features of the Halo-Substituted Materials $[Fe^{III}(5\text{-X-salMeen})_2]Y$: A Cooperative [HS-HS]↔[HS-LS] Spin Transition. *Chem. - A Eur. J.* **2020**, *26* (21), 4766−4779.
(58) Dey, B.; Mondal, A.; Konar, S. Effect of Ligand Field Strength on the Spin Crossover Behaviour in 5-X-salEen (X = Me, Br and OMe) Based Fe(III) Complexes. *Chem. - An Asian J.* **2020**, *15* (11), 1709−1721.
(59) Timken, M. D.; Hendrickson, D. N.; Sinn, E. Dynamics of Spin-State Interconversion and Cooperativity for Ferric Spin-Crossover Complexes in the Solid State. 3. Bis[*N*-(2-(benzylamino)ethyl)-salicylaldiminato]Iron(III) Complexes. *Inorg. Chem.* **1985**, *24* (23), 3947−3955.
(60) *Rigaku XRD*, Rigaku Corporation: Tokyo, Japan, 2018.
(61) *CrysAlisPro*, Rigaku Corporation: Tokyo, Japan, 2019.
(62) Sheldrick, G. M. *Acta Crystallogr., Sect. A: Found. Adv.* **2015**, *71*, 3−8.
(63) Sheldrick, G. M. *Acta Crystallogr., Sect. C: Struct. Chem.* **2015**, *71*, 3−8.
(64) Roos, B. O. The Complete Active Space Self-Consistent Field Method and Its Applications in Electronic Structure Calculations. In *Advances in Chemical Physics*; John Wiley & Sons, Ltd, 1987; pp 399−445. DOI: 10.1002/9780470142943.ch7.
(65) Angeli, C.; Cimiraglia, R.; Malrieu, J.-P. *N*-Electron Valence State Perturbation Theory: A Spinless Formulation and an Efficient Implementation of the Strongly Contracted and of the Partially Contracted Variants. *J. Chem. Phys.* **2002**, *117* (20), 9138−9153.
(66) Neese, F. Software Update: The ORCA Program System—Version 5.0. *Wiley Interdiscip. Rev. Comput. Mol. Sci.* **2022**, *2021*, No. e1606.
(67) Neese, F.; Wennmohs, F.; Becker, U.; Riplinger, C. The ORCA Quantum Chemistry Program Package. *J. Chem. Phys.* **2020**, *152* (22), 224108.
(68) Weigend, F. Accurate Coulomb-Fitting Basis Sets for H to Rn. *Phys. Chem. Chem. Phys.* **2006**, *8* (9), 1057.
(69) Weigend, F.; Ahlrichs, R. Balanced Basis Sets of Split Valence, Triple Zeta Valence and Quadruple Zeta Valence Quality for H to Rn: Design and Assessment of Accuracy. *Phys. Chem. Chem. Phys.* **2005**, *7* (18), 3297.

(70) Atanasov, M.; Aravena, D.; Suturina, E.; Bill, E.; Maganas, D.; Neese, F. First Principles Approach to the Electronic Structure, Magnetic Anisotropy and Spin Relaxation in Mononuclear 3d-Transition Metal Single Molecule Magnets. *Coord. Chem. Rev.* **2015**, *289−290* (1), 177−214.
(71) Lang, L.; Atanasov, M.; Neese, F. Improvement of Ab Initio Ligand Field Theory by Means of Multistate Perturbation Theory. *J. Phys. Chem. A* **2020**, *124* (5), 1025−1037.
(72) Biswas, S.; Mitra, K.; Chattopadhyay, S. K.; Adhikary, B.; Lucas, C. R. Mononuclear Manganese(II) and Manganese(III) Complexes of N_2O Donors Involving Amine and phenolate Ligands: Absorption Spectra, Electrochemistry and Crystal Structure of $[Mn(L3)_2](ClO_4)$. *Transit. Met. Chem.* **2005**, *30* (4), 393−398.
(73) Gildea, B.; Harris, M. M.; Gavin, L. C.; Murray, C. A.; Ortin, Y.; Müller-Bunz, H.; Harding, C. J.; Lan, Y.; Powell, A. K.; Morgan, G. G. Substituent Effects on Spin State in a Series of Mononuclear Manganese(III) Complexes with Hexadentate Schiff-Base Ligands. *Inorg. Chem.* **2014**, *53* (12), 6022−6033.
(74) Liu, Z.; Liang, S.; Di, X.; Zhang, J. A Manganese(III) Complex That Exhibits Spin Crossover Behavior. *Inorg. Chem. Commun.* **2008**, *11* (7), 783−786.
(75) Clegg, J. K.; Cremers, J.; Hogben, A. J.; Breiner, B.; Smulders, M. M. J.; Thoburn, J. D.; Nitschke, J. R. A Stimuli Responsive System of Self-Assembled Anion-Binding $Fe_4L_6^{8+}$ Cages. *Chem. Sci.* **2013**, *4* (1), 68−76.
(76) Kulmaczewski, R.; Trzop, E.; Kershaw Cook, L. J.; Collet, E.; Chastanet, G.; Halcrow, M. A. The Role of Symmetry Breaking in the Structural Trapping of Light-Induced Excited Spin States. *Chem. Commun.* **2017**, *53* (99), 13268−13271.
(77) Chilton, N. F.; Anderson, R. P.; Turner, L. D.; Soncini, A.; Murray, K. S. PHI: A Powerful New Program for the Analysis of Anisotropic Monomeric and Exchange-coupled polynuclear d - and f -block Complexes. *J. Comput. Chem.* **2013**, *34* (13), 1164−1175.
(78) Cole, K. S.; Cole, R. H. Dispersion and Absorption in Dielectrics I. Alternating Current Characteristics. *J. Chem. Phys.* **1941**, *9* (4), 341−351.
(79) Reta, D.; Chilton, N. F. Uncertainty Estimates for Magnetic Relaxation Times and Magnetic Relaxation Parameters. *Phys. Chem. Chem. Phys.* **2019**, *21* (42), 23567−23575.
(80) Blackmore, W. J. A.; Gransbury, G. K.; Evans, P.; Kragskow, J. G. C.; Mills, D. P.; Chilton, N. F. Characterisation of Magnetic Relaxation on Extremely Long Timescales. *Phys. Chem. Chem. Phys.* **2023**, *25* (25), 16735−16744.
(81) Gomez-Coca, S.; Cremades, E.; Aliaga-Alcalde, N.; Ruiz, E. Mononuclear Single-Molecule Magnets: Tailoring the Magnetic Anisotropy of First-Row Transition-Metal Complexes. *J. Am. Chem. Soc.* **2013**, *135* (18), 7010−7018.
(82) Atanasov, M.; Ganyushin, D.; Sivalingam, K.; Neese, F. A Modern First-Principles View on Ligand Field Theory Through the Eyes of Correlated Multireference Wavefunctions. In *Molecular Electronic Structures of Transition Metal Complexes II*; Mingos, D. M. P., Day, P., Dahl, J. P., Eds.; Springer: Berlin, Heidelberg, 2012; pp 149−220. DOI: 10.1007/430_2011_57.
(83) Fitzpatrick, A. J.; Stepanovic, S.; Müller-Bunz, H.; Gruden-Pavlović, M. A.; García-Fernández, P.; Morgan, G. G. Challenges in Assignment of Orbital Populations in a High Spin Manganese(III) Complex. *Dalton Trans.* **2016**, *45* (15), 6702−6708.

https://doi.org/10.1021/acs.inorgchem.4c01317
Inorg. Chem. 2024, 63, 12858−12869

Thermal Jahn-Teller distortion changes and slow relaxation of magnetization in Mn(III) Schiff base complexes

Chantalaksana Chantarangkul,[a] Apinya Patigo,[a] John C. McMurtrie,[b] Rodolphe Clérac,[c] Mathieu Rouzières,[c] Silvia Gómez-Coca,[d] Eliseo Ruiz,[d] Phimphaka Harding,[e] and David J. Harding*[e]*

[a] Functional Materials and Nanotechnology Centre of Excellence, Walailak University, Thasala, Nakhon Si Thammarat, 80160, Thailand.

[b] Queensland University of Technology (QUT), Brisbane, Queensland 4001, Australia

[c] Univ. Bordeaux, CNRS, CRPP, UMR 5031, F-33600 Pessac, France.

[d] Departament de Química Inorgànica i Orgànica, Institut de Recerca de Química Teòrica i Computacional, Universitat de Barcelona, Diagonal 645, 08028 Barcelona, Spain.

[e] School of Chemistry, Institute of Science, Suranaree University of Technology, Nakhon Ratchasima, 30000, Thailand

E-mail: david@g.sut.ac.th or phimphaka@g.sut.ac.th

IR and UV-VIS spectroscopies

Table S1. Spectroscopic data of $[Mn(salRen\text{-}Br)_2]Y$ **1-4**.

	Complex	Wavenumber (cm^{-1})				λ /nm (ε /$M^{-1}cm^{-1}$)
		ν_{N-H}	$\nu_{C=N}$	$\nu_{C=C}$	ν_{anion}	
1	$[Mn(salEen\text{-}Br)_2]ClO_4$	3274	1616	1448	1088	320-360 (shoulder 7100), 400-440 (4700 for **1** and 5600 for **2-4**)
2	$[Mn(salEen\text{-}Br)_2]BF_4$	3301	1618	1448	1055	
3	$[Mn(salBzen\text{-}Br)_2]ClO_4$	3279	1612	1450	1127	
4	$[Mn(salBzen\text{-}Br)_2]BF_4$	3299	1612	1452	1076	

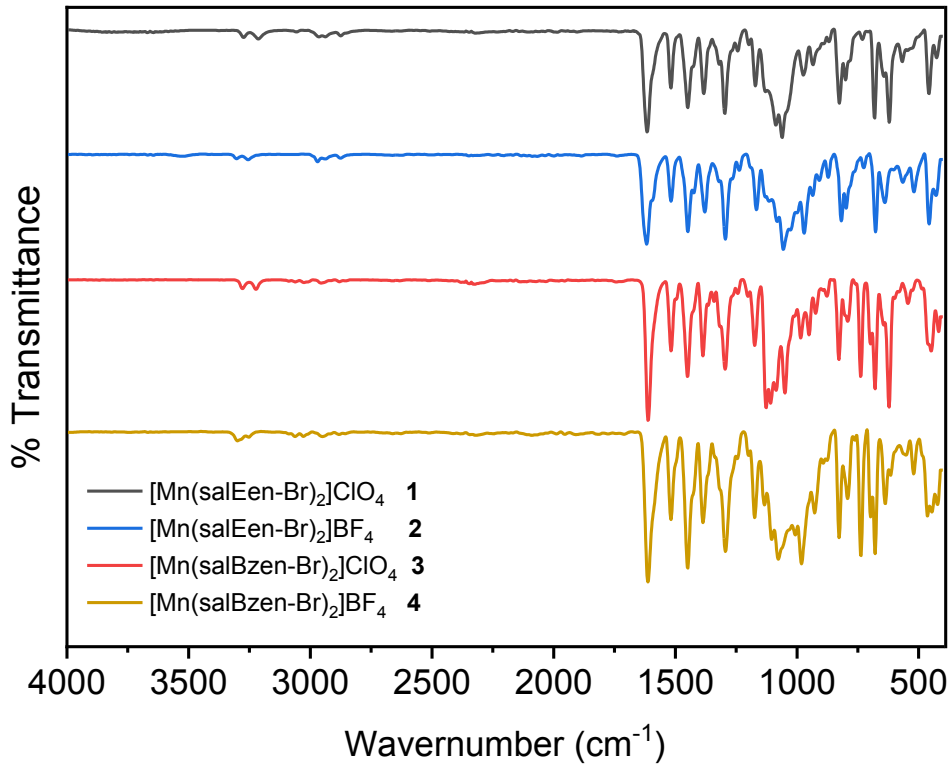

Figure S1. IR spectra (ATR) of **1-4** at room temperature.

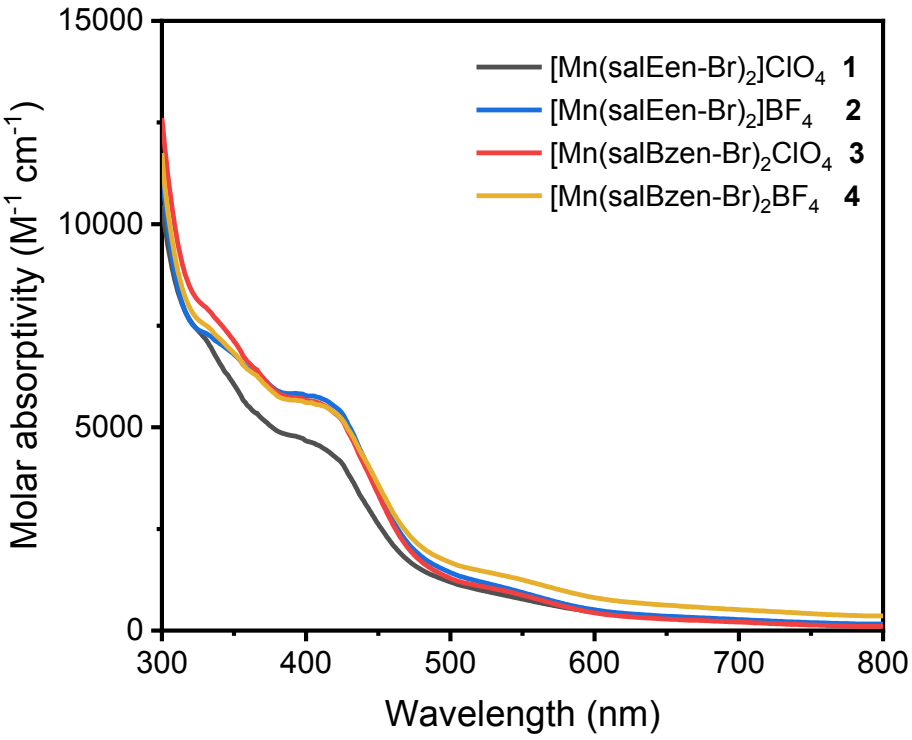

Figure S2. UV-Vis spectra of **1-4** (in CH_2Cl_2 at 0.05 mM) at room temperature.

Thermogravimetric analysis

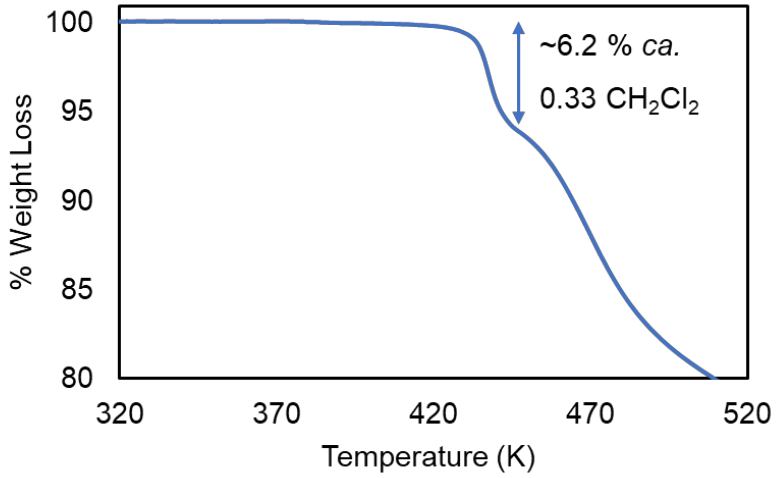

Figure S3. TGA curve for **2**, with the assigned mass loss.

Structural studies

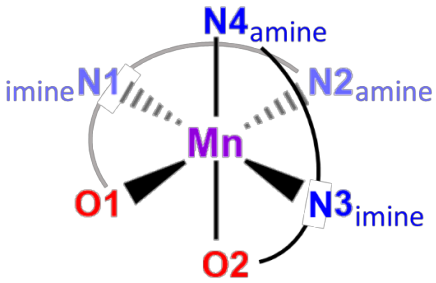

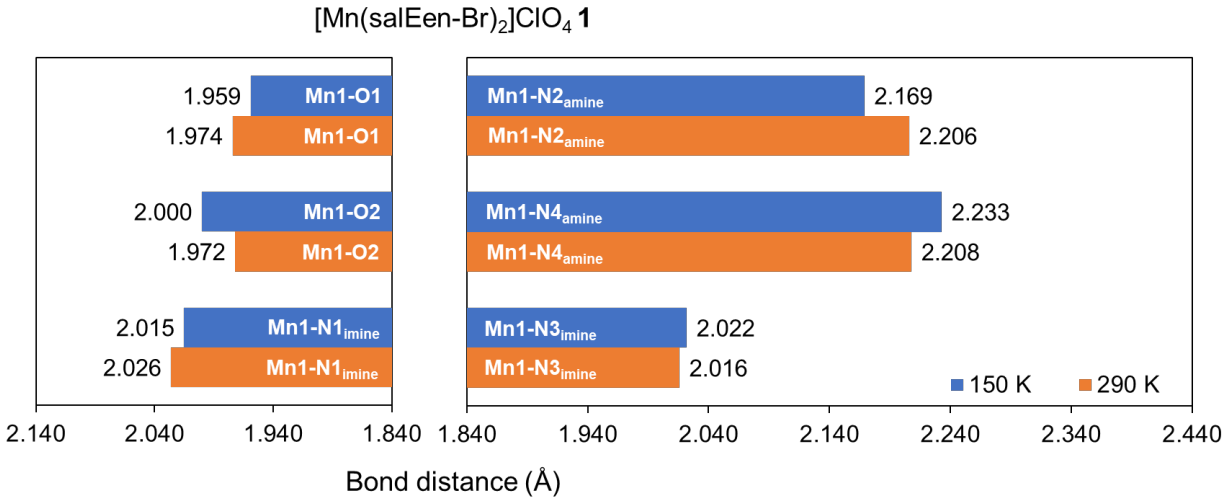

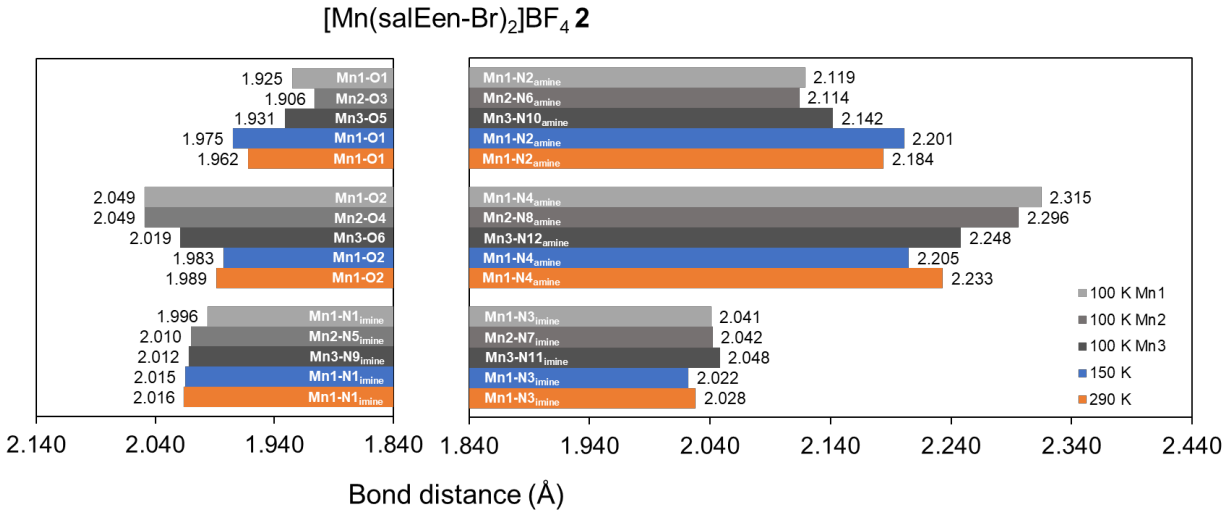

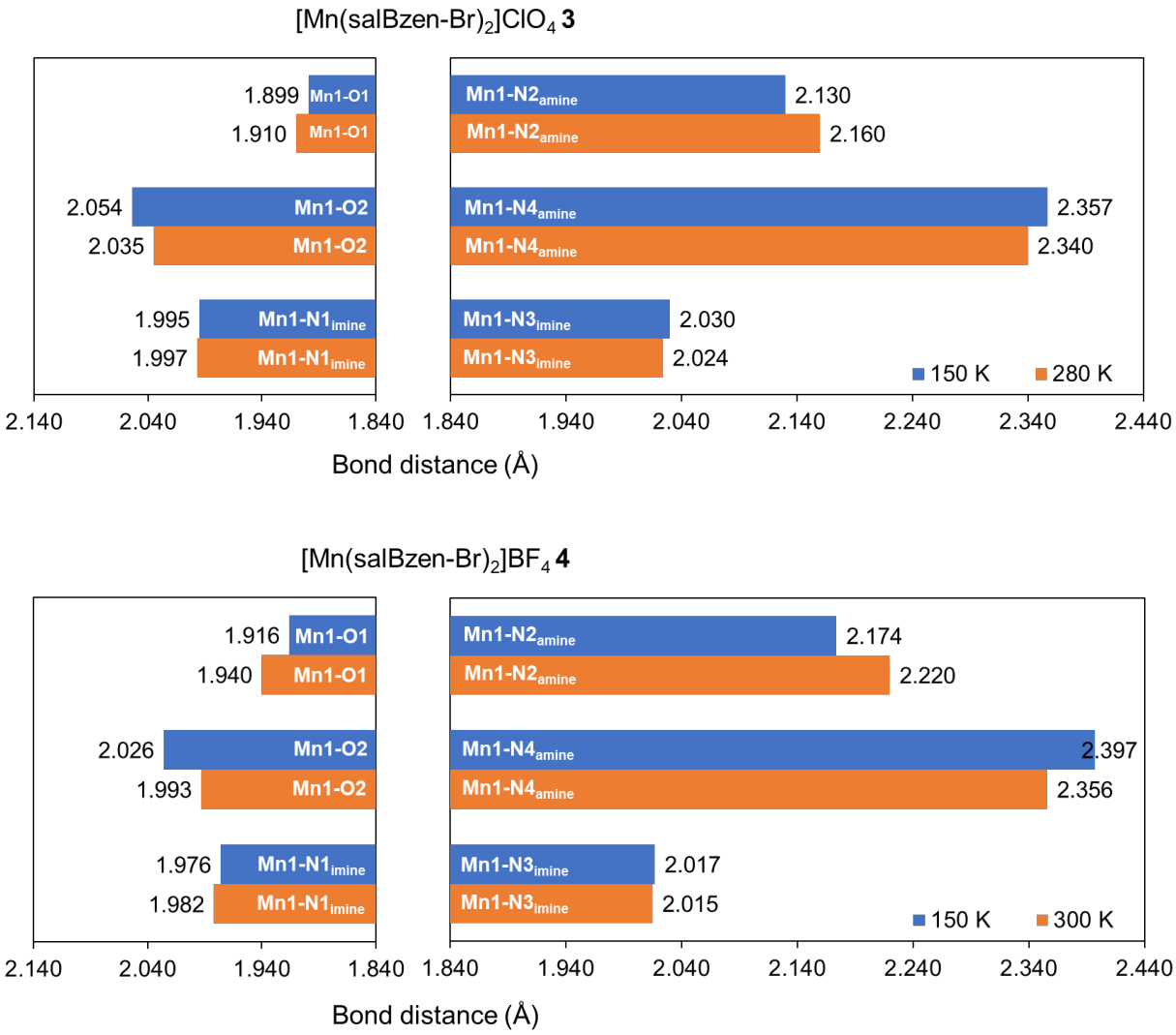

Figure S4. Detailed comparison of the Mn-N/O bond distances of **1**-**4** at high and low temperatures.

Table S2. Bond distances (Å) of [Mn(salRen-Br)$_2$]Y **1-4** (esd values in parentheses).

Bond list	1		2					3		4	
	290 K	150 K	290 K	150 K	100 K			280 K	150 K	300 K	150 K
					Mn1	Mn2	Mn3				
Mn1-O1	1.974(2)	1.959(3)	1.961(5)	1.975(4)	1.925(3)	1.906(3)	1.931(3)	1.910(2)	1.899(2)	1.940(2)	1.916(2)
Mn1-O2	1.972(3)	2.000(3)	1.989(3)	1.983(3)	2.049(3)	2.049(3)	2.019(3)	2.035(2)	2.054(2)	1.993(3)	2.026(2)
Mn1-N1$_{imine}$	2.026(3)	2.015(3)	2.016(4)	2.015(3)	1.996(3)	2.010(3)	2.012(3)	1.997(3)	1.995(3)	1.982(3)	1.976(2)
Mn1-N2$_{amine}$	2.206(3)	2.169(3)	2.184(4)	2.201(3)	2.119(3)	2.114(3)	2.142(3)	2.160(3)	2.130(3)	2.220(3)	2.174(2)
Mn1-N3$_{imine}$	2.016(3)	2.022(3)	2.028(4)	2.022(3)	2.041(3)	2.042(3)	2.048(3)	2.024(3)	2.030(3)	2.015(3)	2.017(2)
Mn1-N4$_{amine}$	2.208(3)	2.233(3)	2.233(4)	2.205(3)	2.315(4)	2.296(3)	2.248(3)	2.340(2)	2.357(2)	2.356(4)	2.397(3)

Magnetic measurements

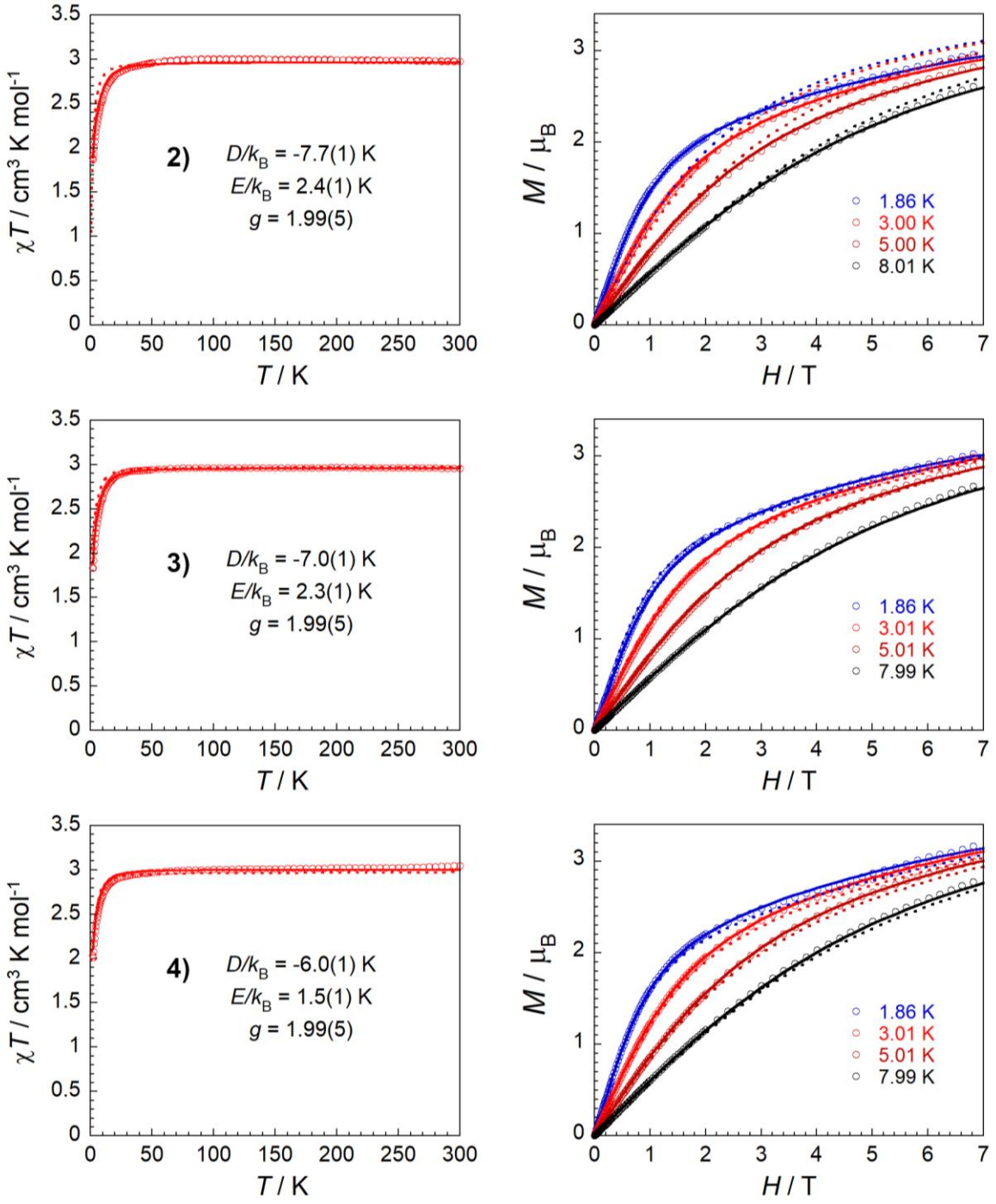

Figure S5. Temperature (T) dependence of the molar susceptibility (χ) at 1000 Oe shown as χT versus T plots (left), and dc-field dependence (H) of the magnetization M below 8 K (right) for **2**, **3** and **4**. Open circles are experimental data, solid lines are best fits (with the final D, E and g values shown in the left plot) from the Phi software (see main text) and dotted lines are theoretical χT versus T and M versus H plots calculated from theoretical approach (see main text).

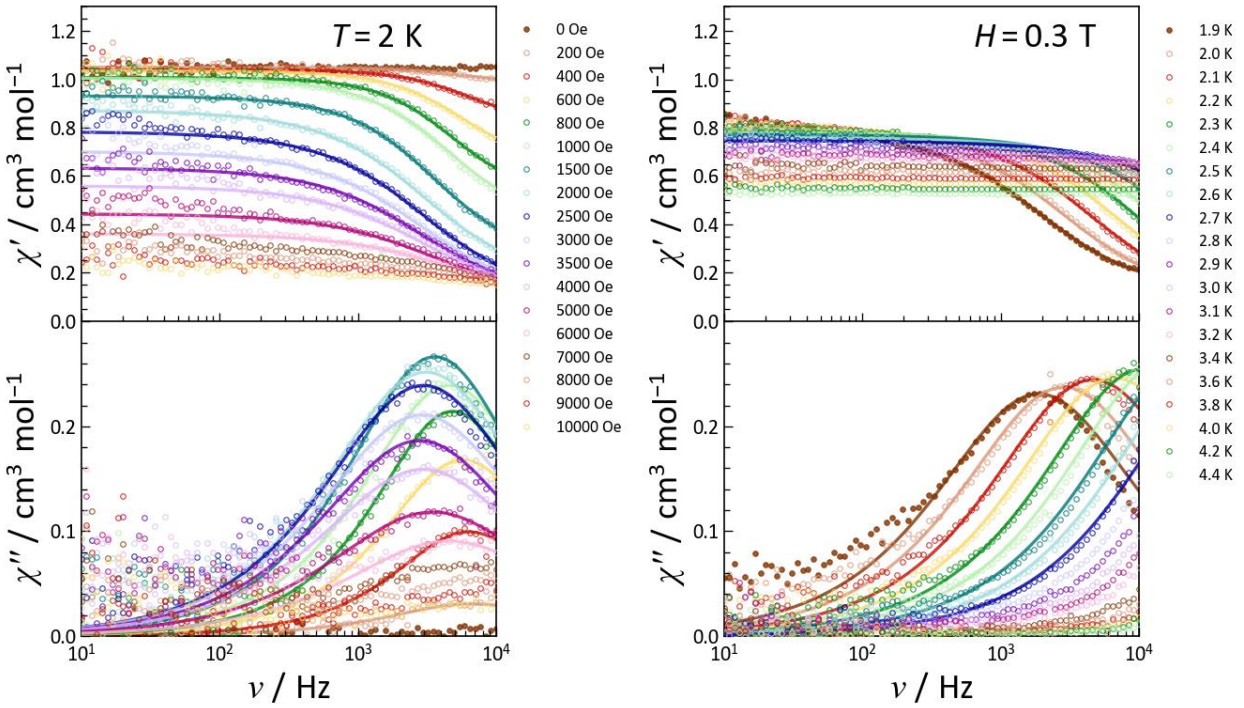

Figure S6. Frequency dependence of the in-phase (top; χ') and out-of-phase (bottom; χ'') components of the ac susceptibility at 2 K and indicated dc field between 0 and 1 T (left) and at 0.3 T and indicated temperatures between 1.9 and 4.4 K for **4**. Solid lines are best fits to the generalized Debye model.

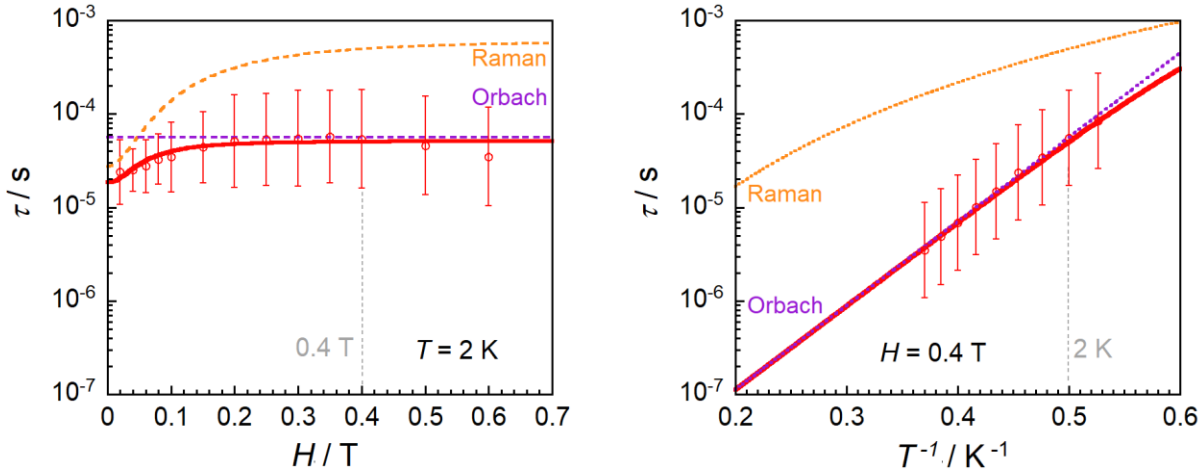

Figure S7. Left: Field dependence of the relaxation time (plotted as τ vs H in semi-logarithm scale) at 2 K for **4**. Right: Temperature dependence of the relaxation time (plotted as τ vs T^{-1} in semi-logarithm scale) at 0.4 T for **4**. Open circles are the experimental data and bars denote ESDs of distribution of times from the generalized Debye model. Solid lines are the result of the best global simulation as discussed in the text. Dotted lines are Raman (orange), and Orbach (purple) components of the model.

Table S3. Reported magnetic parameters for mononuclear Mn(III) SMMs.

Complex	D [cm^{-1} (K)]	E [cm^{-1} (K)]	Δ_{eff} [cm^{-1} (K)]	τ_0 [s]	H [Oe]	Ref.
$Ph_4P[Mn(opbaCl_2)(py)_2]$	-3.42 (-4.92)[a]	-0.15 (-0.21)[a]	12.6 (18.1)	1.2×10^{-7}	1000	1
[Mn(5-TMAM(*R*)-salmen)$(H_2O)Co(CN)_6$] $\cdot 7H_2O \cdot$MeCN	-3.3 (-4.7)[a]	0[a]	11.5 (16.5)	2.9×10^{-7}	4500	2
$[Mn\{(OPPh_2)_2N\}_3]$	-3.4 (-4.9)[a]		8.3 (11.9)	0.5×10^{-7}	2250	3
			8.0 (11.5)	0.6×10^{-7}	2500	
			8.2 (11.8)	0.6×10^{-7}	2900	
			7.4 (10.6)	1.0×10^{-7}	3500	
			7.0 (10.1)	1.4×10^{-7}	4000	
$[Mn(dbm)_3]$	-4.55 (-6.55)[a]	0.28 (0.40)[a]	11.5 (16.5)	2.3×10^{-7}	2000	4
$[Mn(dbm)_2(DMSO)_2]ClO_4$	-3.42 (-4.92)[b]	0.74 (1.06)[b]	16.8 (24.2)	9.4×10^{-9}	1500	
$[Mn(dbm)_2(py)_2]ClO_4$	-4.5 (-6.5)[a]	-0.40 (-0.58)[a]	18.5 (26.6)	9.2×10^{-8}	1500	
$Na_5[Mn(L\text{-}tart)_2] \cdot 12H_2O$	-3.23 (-4.65)[a]	0.03 (0.04)[a]	5.4 (7.8)	2.3×10^{-6}	500	5
			9.0 (12.9)	3.4×10^{-6}	2000	
			9.9 (14.2)	6.4×10^{-6}	5000	
[Mn(TPP)(3,5-$Me_2pyNO)_2$]$ClO_4 \cdot CH_3CN$	-3.82 (-5.5)[a]	0.16 (0.23)[a]	15.5 (22.3)	1.2×10^{-8}	1000	6
			15.3 (22.0)	1.9×10^{-8}	2000	
			15.6 (22.4)	1.2×10^{-8}	3000	
			15.5 (22.3)	2.0×10^{-8}	4000	
{Na[Mn(CH_3OH)(Hvanox)(vanox)(HCOO)]$\cdot CH_3OH$}	-3.54 (-5.09)[b]	-0.20 (-0.29)[b]	12.9 (18.6)	6.4×10^{-8}	2000	7
$[Mn(3\text{-}OEt\text{-}salme)_2]BPh_4$	-4.73 (-6.81)[b]	0.09 (0.13)[b]	7.1 (10.2)	1.5×10^{-6}	2000	8
$[Mn(salBzen\text{-}Br)_2]ClO_4$	-4.87 (-7.01)[b]	1.60 (2.30)[b]	19.5 (27.8)	1.8×10^{-9}	3000	This
$[Mn(salBzen\text{-}Br)_2]BF_4$	-4.17 (-6.00)[b]	1.04 (1.50)[b]	14.6 (20.7)	1.8×10^{-9}	4000	work

$H_4opbaCl_2$ = *N,N′*-3,4-dichloro-ortho-phenylenebis(oxamic acid), py= pyridine, 5-TMAM-(*R*)-salmen = (*R*)-*N,N′*-(1-methylethylene)bis(5-trimethylammoniomethylsalicylideneiminate, $(OPPh_2)_2HN$= tetraphenyl imido-diphosphinic acid, Hdbm=dibenzoylmethane, L=(R)-*N,N′*-(1-methylethylene)bis[(5-trimethyl ammoniomethyl)salicylideneiminate], L-tart = L-tartrate, H_2TPP= 5,10,15,20-tetraphenylporphyrin, Me_2pyNO=dimethylpyridine *N*-oxide, H_2vanox = *o*-vanillinoxime, salme = *N*-methyl-*N*-(3-aminopropyl)-salicylaldiminate, and salBzen-Br = 2-{[2-(benzylamino)ethylimino]methyl}-4-Br-phenol.

[a] Obtained by HFEPR spectroscopy. [b] Obtained by fitting the dc magnetic data.

Electronic structure calculations

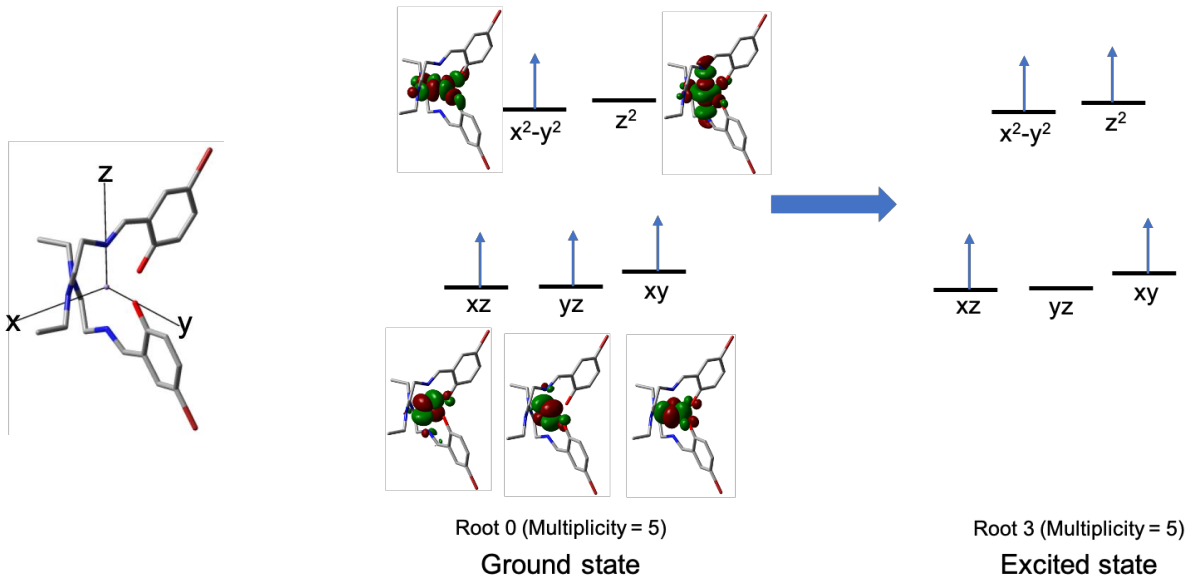

Figure S8. Calculated orientations of $[Mn(salEen\text{-}Br)_2]^+$ (**1**$^+$ and **2**$^+$), with black lines representing cartesian (x,y,z) axes (left). The energy order of the (4,5) active space d orbitals for the $[Mn(salEen\text{-}Br)_2]^+$ complex in its ground state and first excited state of the main *D*-tensor contribution give positive *D* value (right). The third ground state (Root 3) is the one with the largest contribution to the D value.

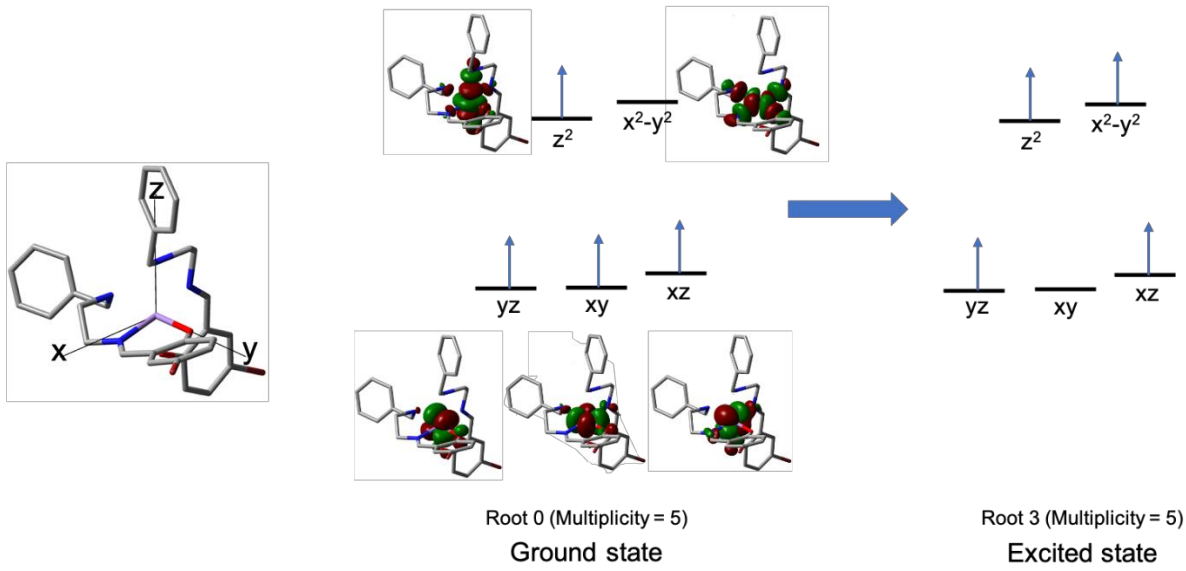

Figure S9. Calculated orientations of $[Mn(salBzen\text{-}Br)_2]^+$ (**3**$^+$ and **4**$^+$), with black lines representing cartesian (x,y,z) axes (left). The energy order of the (4,5) active space d orbitals for the $[Mn(salBzen\text{-}Br)_2]^+$ complex in its ground state and first excited state of the main *D*-tensor contribution give negative *D* value (right). The third ground state (Root 3) is the one with the largest contribution to the D value.

Table S4. Calculated AILFT d orbital energies using the NEVPT2 method.

$[Mn(salEen\text{-}Br)_2]^+$ **1**$^+$		$[Mn(salEen\text{-}Br)_2]^+$ **2**$^+$		$[Mn(salBzen\text{-}Br)_2]^+$ **3**$^+$		$[Mn(salBzen\text{-}Br)_2]^+$ **4**$^+$	
d orbital	**Energy [cm^{-1} (K)]**	**d orbital**	**Energy [cm^{-1} (K)]**	**d orbital**	**Energy [cm^{-1} (K)]**	**d orbital**	**Energy [cm^{-1} (K)]**
xz	0.0	xz	0.0	xz	0.0	xz	0.0
yz	341.5 (491.3)	yz	335.3 (482.4)	xy	945.3 (1360.1)	xy	1374.4 (1977.5)
xy	1812.4 (2607.7)	xy	1811.0 (2605.6)	yz	1971.2 (2836.1)	yz	1952.9 (2809.8)
x^2-y^2	13818.0 (19881.1)	x^2-y^2	13988.9 (20127.0)	z^2	12257.6 (17636.1)	z^2	11990.1 (17251.2)
z^2	18031.2 (25943.0)	z^2	17916.0 (2577.3)	x^2-y^2	19580.1 (28171.6)	x^2-y^2	19434.0 (27961.4)

References

(1) Vallejo, J.; Pascual-Álvarez, A.; Cano, J.; Castro, I.; Julve, M.; Lloret, F.; Krzystek, J.; De Munno, G.; Armentano, D.; Wernsdorfer, W.; Ruiz-García, R.; Pardo, E. Field-Induced Hysteresis and Quantum Tunneling of the Magnetization in a Mononuclear Manganese(III) Complex. *Angew. Chemie - Int. Ed.* **2013**, *52* (52), 14075–14079. https://doi.org/10.1002/anie.201308047.

(2) Ishikawa, R.; Miyamoto, R.; Nojiri, H.; Breedlove, B. K.; Yamashita, M. Slow Relaxation of the Magnetization of an Mn^{III} Single Ion. *Inorg. Chem.* **2013**, *52* (15), 8300–8302. https://doi.org/10.1021/ic401351w.

(3) Grigoropoulos, A.; Pissas, M.; Papatolis, P.; Psycharis, V.; Kyritsis, P.; Sanakis, Y. Spin-Relaxation Properties of a High-Spin Mononuclear $Mn^{III}O_6$-Containing Complex. *Inorg. Chem.* **2013**, *52* (22), 12869–12871. https://doi.org/10.1021/ic402042e.

(4) Chen, L.; Wang, J.; Liu, Y. Z.; Song, Y.; Chen, X. T.; Zhang, Y. Q.; Xue, Z. L. Slow Magnetic Relaxation in Mononuclear Octahedral Manganese(III) Complexes with Dibenzoylmethanide Ligands. *Eur. J. Inorg. Chem.* **2015**, *2015* (2), 271–278. https://doi.org/10.1002/ejic.201402964.

(5) Craig, G. A.; Marbey, J. J.; Hill, S.; Roubeau, O.; Parsons, S.; Murrie, M. Field-Induced Slow Relaxation in a Monometallic Manganese(III) Single-Molecule Magnet. *Inorg. Chem.* **2015**, *54* (1), 13–15. https://doi.org/10.1021/ic5024136.

(6) Pascual-Álvarez, A.; Vallejo, J.; Pardo, E.; Julve, M.; Lloret, F.; Krzystek, J.; Armentano, D.; Wernsdorfer, W.; Cano, J. Field-Induced Slow Magnetic Relaxation in a Mononuclear

Manganese(III)-Porphyrin Complex. *Chem. - A Eur. J.* **2015**, *21* (48), 17299–17307. https://doi.org/10.1002/chem.201502637.

(7) Liu, Y. M.; Liu, Z. Y.; Yang, E. C.; Zhao, X. J. Field-Induced Slow Relaxation of a Manganese(III)-Based Single-Ion Magnet. *Inorg. Chem. Commun.* **2017**, *77*, 27–30. https://doi.org/10.1016/j.inoche.2017.01.030.

(8) Realista, S.; Fitzpatrick, A. J.; Santos, G.; Ferreira, L. P.; Barroso, S.; Pereira, L. C. J.; Bandeira, N. A. G.; Neugebauer, P.; Hrubý, J.; Morgan, G. G.; Van Slageren, J.; Calhorda, M. J.; Martinho, P. N. A Mn(III) Single Ion Magnet with Tridentate Schiff-Base Ligands. *Dalt. Trans.* **2016**, *45* (31), 12301–12307. https://doi.org/10.1039/c6dt02538b.